Quaternary Science Reviews 170 (2017) 26–44

Contents lists available at ScienceDirect

Quaternary Science Reviews

journal homepage: www.elsevier.com/locate/quascirev

Subglacial till formation: Microscale processes within the subglacial shear zone

Jane K. Hart

Geography and Environment, University of Southampton, SO17 1BJ, UK

ARTICLE INFO

Article history:
Received 17 March 2017
Received in revised form
13 June 2017
Accepted 22 June 2017

Keywords:
Present
Glaciology
Western Europe
Geomorphology
Glacial
Till genesis
Subglacial processes
Subglacial deformation
Thin section

ABSTRACT

This was a study of subglacial deformation till genesis from a modern temperate glacier, at Skálafellsjökull, Iceland. Detailed microscale properties of till samples (from Scanning Electron Microscope [SEM] and thin section analysis) were examined from a glacial site with *in situ* subglacial process monitoring and an exposed subglacial surface in the foreland. Two lithofacies were examined, a grey sandy till derived from the ash and basalt, and a silty reddish brown till derived from oxidized paleosols and/or tephra layers. These also represented a clay-content continuum from low (0.3%) to high (22.3%). The evolution from debris to subglacial till was investigated. This included a reduction in grain-size (21% for grey lithology, 13% reddish brown lithology), and reduction in rounding (RA) (32% for the grey lithology, 26% for the reddish brown lithology), and the quantification and analysis of the different grain erosion/comminution processes in the resultant till. It was shown that the microstructures within a till were dependent on shear strain and glaciological conditions (deformation history). The low clay content tills were dominated by linear structures (lineations and boudins, and anisotropic microfabric) whilst the higher clay content tills were dominated by rotational structures (turbates and plaster, and isotropic microfabric). These results are important in our understanding of the formation of both modern and Quaternary tills and informs our reconstruction of past glacial dynamics.

1. Introduction

Temperate glacier motion is due to creep, sliding and subglacial deformation; and so subglacial hydrology and sediment deformation play a key role in modulating glacier behaviours (Boulton and Jones, 1979; Murray and Dowdeswell, 1992). The study of their interaction is vital for any prediction of glacier response to climate change, and the reconstruction of past glacier behaviour from glacial sediments. Understanding the subglacial environment must include a combination of *in situ* subglacial experiments (Fischer and Clarke, 2001; Murray and Porter, 2001; Hart et al., 2011a), geophysical and geodetic survey (Woodward et al., 2003; Smith et al., 2007; Hart et al., 2011b), geotechnical experiments (Kamb, 1991; Iverson et al., 1998; Sane et al., 2008; Altuhafi et al., 2009; Iverson, 2010) and sedimentology (Hart and Rose, 2001; Evans et al., 2006; Ó Cofaigh et al., 2011; Trommelen et al., 2014). Such studies have illustrated that the processes within the subglacial environment can vary rapidly on both a spatial and temporal scale, with 20–85% of glacier motion occurring in a subglacial deforming layer (typically to 0.3 m depth) (Truffer et al., 2000; Boulton et al., 2001; Cuffey and Paterson, 2010).

The key driver for subglacial till sedimentation is pore-water pressure (Alley et al., 1986; Boulton and Hindmarsh, 1987; Brown et al., 1987; van der Meer et al., 2003; Iverson, 2010). Where pore-water pressures are very low, the till cannot be deformed. At intermediate pore-water pressures, subglacial sediments are deformed and behave as a shear zone (Hart and Boulton, 1991; Benn and Evans, 1996). At extremely high pore-water pressures, there is ice-bed decoupling and/or shallow deformation (Fischer and Clarke, 1997; Engelhardt and Kamb, 1998; Iverson et al., 1999; Boulton et al., 2001; Damsgaard et al., 2013). Hart et al. (2011a) was able to demonstrate, from *in situ* wireless probe data from Briksdalsbreen, Norway, the deformation patterns (discussed above) forming in response to an annual cycle of pore-water pressure changes. The resultant till is a mixture of all these processes.

Till is a granular material with complex geotechnical behaviour (see detailed discussions in Menzies, 2012; and Damsgaard et al., 2016) and involves the movement of particles at both microscopic

E-mail address: jhart@soton.ac.uk.

http://dx.doi.org/10.1016/j.quascirev.2017.06.021
0277-3791/

(clast and matrix) and macroscopic (bulk rheology) scale. Although there have been debates about till behaviour, between a linear viscous model (Alley et al., 1986; Boulton and Hindmarsh, 1987) or plastic behaviour (Kamb, 1991; Tulaczyk et al., 2000); more recently it has been argued that there is a continuum in behaviour from 'stick' (little motion) to 'creep' (pre-failure, nonlinear deformation) to 'slip' (plastic failure) (Hindmarsh, 1997; Sane et al., 2008; Altuhafi et al., 2009; Hart et al., 2011a; Damsgaard et al., 2016). During deformation, the particles (both grains and matrix) are rearranged, leading to grain erosion (comminution) (Gjessing, 1965; Hooke and Iverson, 1995; van der Meer et al., 2003; Hart, 2006a) which itself makes a contribution (due to changes in grain size and arrangement) to the deformation process.

The aim of this study was to investigate the formation of subglacial deformation till from beneath a modern glacier. To do this, sedimentological techniques (SEM, thin section and microfabric) are used alongside data collected from the unique Glacsweb *in situ* subglacial wireless probes (Hart et al., 2006; Martinez and Hart, 2010). There are three specific aims: i) the comparison of erosional characteristics between the debris and the subglacial tills; ii) the investigation of the styles of deformation (strain patterns) within the till; and iii) the influence of lithology and particularly clay content, on subglacial processes. The study of till genesis requires an understanding of both temporal changes (from modern studies) and spatial changes (often easier to determine from Quaternary studies), so that till can be actively used as a tool for the reconstruction of former glacier behaviour.

2. Skálafellsjökull

2.1. Field site

The study was undertaken at Skálafellsjökull, Iceland (Fig. 1). This is an outlet glacier of the Vatnajökull icecap resting on Upper Tertiary grey basalts with intercalated sediments (oxidized paleosols and/or tephra layers) (Jóhannesson and Sæmundsson, 1998). The area of the glacier is approximately 100 km^2 with a length of 25 km (Sigurðsson, 1998). In order to study the till sedimentology we collected the till from two locations (Fig. 1b). One site that has been the focus of wireless *in situ* subglacial experiments (Site A) (Hart et al., 2015; Martinez et al., 2017); and a second from the proglacial foreland where there was an exposed subglacial surface (Site B). At the glacier site (Site A), bulk samples of supraglacial, englacial and proglacial material were collected alongside subglacial samples (collected via borehole). A second site was investigated in the foreland because it provided access to a recently exposed subglacial surface, where bulk and undisturbed subglacial till samples were collected from both a push moraine and a flute. The choice of two sites enabled us to use a wide range of sampling techniques and compare *in situ* subglacial processes and recently deposited subglacial till.

2.2. Site A

Site A (792 m a.s.l.) was chosen for subglacial monitoring because the glacier was flat and relatively crevasse free. Clast-rich till and small push moraines (<1 m high) were present along the greater part of the glacier margin. Numerous englacial debris bands and debris cones were also visible on the glacier surface throughout the glacier ablation zone (Figs. 1c and 2). These typically consisted of thin clast-rich layers (1–2 cm thick) with 4–10 layers in approximately 1 m thickness (Fig. 2). Almost all the clasts were less than 1 cm in length (a-axis). Towards the margin, there were two sites where the debris-rich layers contained small lenses (a-axis less than 1 cm) of reddish brown clay-rich debris.

At this site, it has been shown from borehole and Ground Penetrating Radar (GPR) studies that the glacier rests on a till base, which comprises a patchwork of different till strengths (Hart et al., 2015). The till/bedrock interface is clearly seen on the GPR, and is close to the surface (less than 1 m) at the margin and inclines beneath the glacier at approximately 30° degrees, so that at 150 m from the margin the till is approximately 2 m thick.

In addition, a wireless subglacial sensor network was installed to measure subglacial processes (Hart and Martinez, 2006; Martinez and Hart, 2010; Martinez et al., 2017). Three wireless *in situ* probes were deployed in the till in 2008. In order to insert probes into the till, the boreholes were drilled to the base of the glacier and the presence of till checked with the video camera. If till was present it was hydraulically excavated (Blake et al., 1992) by maintaining the jet at the bottom of the borehole for an extended period of time. The probes were then lowered into this space, enabling the till to subsequently close in around them. The measured depth of the probes within the till is not known, but is approximated at 0.1–0.2 m beneath the glacier base, estimated from video footage of the till excavation at ice/till interface prior to deployment. The probes were deployed where the ice was 60 m thick and approximately 100 m from the glacier margin.

The Glacsweb probes show that throughout the year, the till was dominated by either stable high water pressure (>90% water pressure as a percentage of glacier depth), or variable water pressures (typically 67–86% water pressure as a percentage of glacier depth) with regular patterns of stick-slip motion (Hart et al., 2015).

2.3. Site B

Site B (60 m a.s.l.) was dominated by flutes and moraines. In the south west of the area the moraines were 50–100 m long and 1–3 m high, with a proximal slope of 10–20° (located along the transect shown in Fig. 1d). Each moraine comprised an upper clast-rich till (0.2 m thick), and a lower unit comprising layers of silt, sand and gravel (Fig. 3). Samples were taken from three moraines located between 40 and 163 m (along the transect) from the 2008 glacier margin. At sites B1-3, within the lower laminated unit, were small (0.15 m high) folds, kink folding (0.1 m high), brittle faulting (Fig. 3) and possible water escape structures.

To the north east of the transect, the foreland comprises a series of flutes and streamlined bedrock (with no underlying proglacial deposits). Site B4 was an exposure of reddish brown till (35 m from the 2008 margin, 175 m east of the transect) in a fluted area. This till lithofacies was also observed within three adjacent flutes (approximate size, 0.7 m high, 0.6 m wide, over 100 m long).

At the 2008 glacier margin, a saturated fluted till surface was being exposed. Throughout the foreland, till depth was variable (ranging from 0 to 3 m) and in places the bedrock was exposed relatively close to the surface, either as small streamlined outcrops (up to 2 m in area) or larger crags.

2.4. Recent glacier movement and till depositional setting

The recent changes in the position of the glacier margin are recorded from air photographs since 1945, Landsat 7 (Google Earth) 2000 image, Cnes/Spot 2013 image and measurement in the field 2008. At the south eastern margin (Site B), Skálafellsjökull retreated from 1945 to 1978 at approximately 24 m a^{-1}; then advanced until 2000 at approximately 6 m a^{-1}, and subsequently retreated at 19 m a^{-1} between 2000 and 2008 and 37 m a^{-1} between 2008 and 2013 (Fig. 1a). The 1978 air photograph shows the minimum glacier position, and during this time there was a large proglacial lake (414 m × 143 m) at the glacier margin. This lake was also present in the 1982 and 1989 air photographs, although becoming smaller

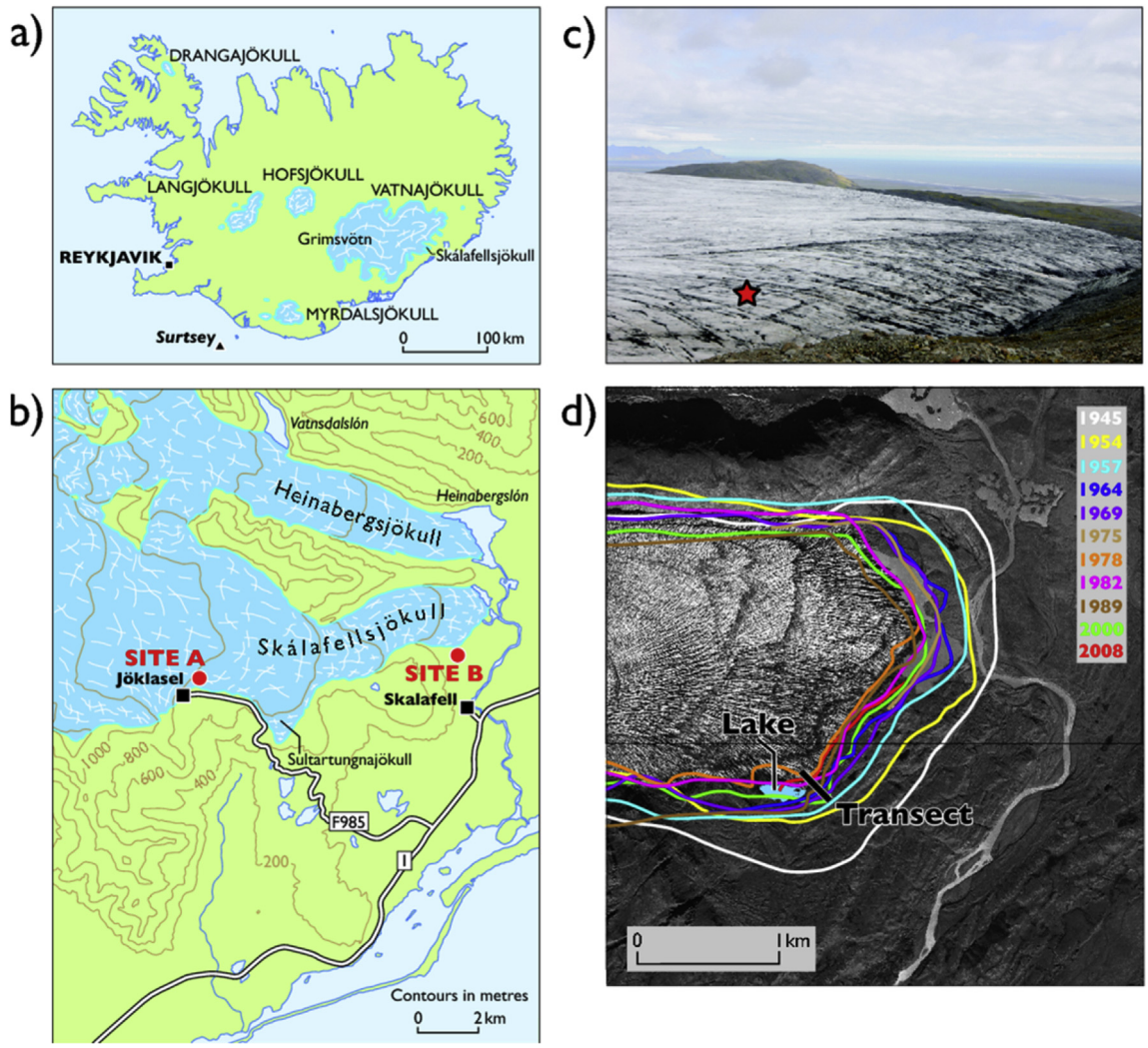

Fig. 1. a) Location of Skálafellsjökull in Iceland; b) Detail of the site with two study sites A and B marked; c) photograph of the glacier showing Site A marked with a star (view to the SE); d) 1978 air photograph of the glacier margin, overlain with lines representing glacier fluctuations from 1945 to 2008. The locations of the Site B transect and the southern proglacial lake (observed in the 1978, 1982 and 1989 air photographs) are also marked.

over time, but it was not visible in the 2000 image nor observed in the field in 2008 or 2015.

It is suggested that the two layered sequence at sites B1-3 comprises a lower stratified unit formed within the lake, which was subsequently overridden by the ice between 1989 and 2000, during which time a subglacial till was deposited. Although detailed discussion of the formation of the moraines is beyond the scope of this paper, it is suggested this two layered sequence was then subsequently stacked during proglacial glaciotectonic deformation during the final re-advance in 2000. These push moraines are similar to those described by Humlum (1985) and Kruger (1985) at Höfabrekkujökull, Iceland, where relatively thin slices of material, facilitated by lubrication along the bedding planes of the stratified sediments (Hart, 1990; van der Wateren, 1995; Phillips and Merritt, 2008), were fractured into a series of thrust sheets.

Although the samples were collected between 25 and 110 m with respect to the 2000 margin, this is probably the result of the final proglacial stacking. Initial subglacial deposition could have occurred approximately 280–25 m (given a maximum compression of 50%) from the margin.

Most of the remainder of the foreland (outside of the area around the lake and transect shown in Fig. 1d) is comprised of flutes, streamlined bedrock and small annual push moraines (Chandler et al., 2016). Site B4 was within this area. The age of the reddish-brown till found within the flute at Site B4 is not known, although it is situated 200 m upglacier of the 2000 limit, and may also have been formed during the 1978–2000 advance.

The western side (Site A) was more stable and marginal positions were measured with dGPS in 2008, 2011, 2012 and 2014, and over this time period has retreated at approximately 4.5 m a^{-1}. The small push moraines at the margin were comprised mostly subglacial till that had been pushed up from beneath the glacier (Price, 1970; Sharp, 1984; Evans and Twigg, 2002). The subglacial samples were all taken from approximately 100 m from the margin.

In summary, the samples collected represent different pathways of material within the glacial system. The englacial debris from Site A represents supraglacial sources of material (weathered from the bedrock, or directly from ash fall) combined with subglacial sources transported by englacial compressive shear planes to the surface. Subglacial material was collected from beneath the glacier and inside a push moraine at Site A, and from the foreland (with a moraine and flute) at Site B. The source of the subglacial material at Site A and B4 was the bedrock, whilst Sites B1-3 overlaid proglacial sediments (a high percentage of which would have originated from

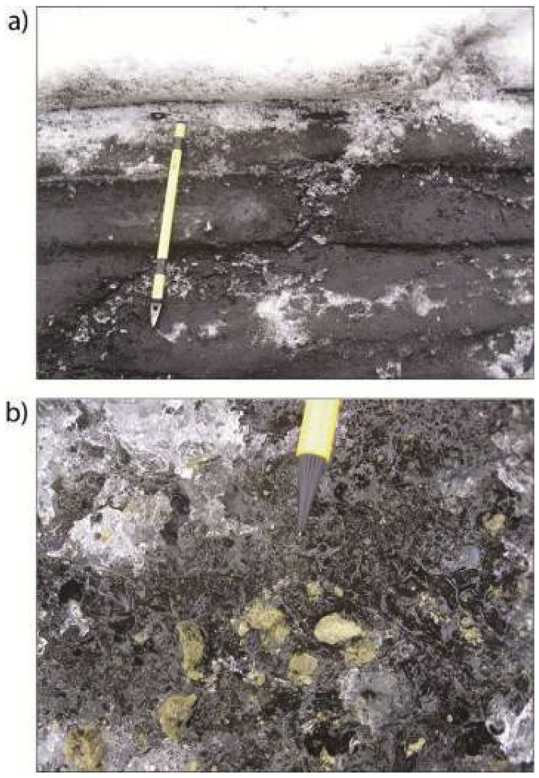

Fig. 2. Photographs to show the nature of the debris bands on the glacier surface: a) typical debris band with grey debris (ice axe 0.7 m long); b) reddish brown clay-rich clasts (a-axis approximately 1 cm) outcropping from a thin clast layer, within a debris band unit.

the subglacial system), and we assume that all the subglacial tills were deposited within 300 m of the margin.

3. Methodology

3.1. Sample collection

Bulk samples were collected from the surface of the glacier (Site A) and the proglacial area (Sites A and B). Till was also collected from the base of five of the boreholes (drilled with a Kärcher HDS1000DE hot water drill) with a subglacial sediment sampler attached to a subglacial percussion hammer (Blake et al., 1992; Rose and Hart, 2008). Undisturbed samples were also collected from the foreland (Site B) in metal Kubeina tins measuring 8 × 6 × 4 cm, alongside bulk samples (Table 1). .

Grain size analysis was undertaken on the bulk and borehole samples (apart from SK12 where the sample was too small, and so was used instead for SEM analysis). Samples representing the different locations (englacial or subglacial) and lithologies (grey or reddish-brown) were then examined by SEM (all the borehole samples were of a similar grey lithofacies). The undisturbed samples were used for thin section analysis..

3.2. Grain size

The grain size composition of the samples was determined through a combination of dry sieving and laser granulometry, and then examined using the GRADISTATv5 programme (Blott and Pye, 2001, 2006). The mean grain size was calculated using the Folk and Ward method (1957) (which takes the mean grain diameter of the 16th, 50th and 84th cumulative percentile).

3.3. SEM

Small samples were mounted on stubs and coated with gold and analysed with a LEO1450VP scanning electron microscope. They were analysed with X-ray elemental mapping (at x 100 or x 150 scale) to measure the intensity levels of silicon and aluminium. Next an IMIX Image processing package was used to analyse each pixel of the image to isolate the quartz grains. The surface textures of the quartz grains were examined at a higher magnification and were analysed based on the techniques proposed by Mahaney et al. (1996). This involves selecting twenty five quartz grains per sample and identifying the various different textures (morphological and mechanical) of each grain, according to a standardised table of features. The original surface (prior to glacial comminution) can be identified, and an estimation of its area (compared with the whole grain area) can be computed (based on the method of Mahaney et al., 1996; Mahaney and Kalm, 2000; Hart, 2006b). At Skálafellsjökull the original surface was relatively straightforward to identify it was very distinctive, comprising either ash (Fig. 4a and b) (grey lithofacies) or clay (Fig. 4l) reddish brown lithofacies. Roundness was also measured, using the Powers (1953) method, and from this the RA value (percentage of clasts that are 'very angular' and 'angular'; Benn and Ballantyne, 1993) was calculated. In addition, the a-axis of the grains was measured.

3.4. Micromorphology

The samples were prepared and mounted on glass slides using the method of Carr and Lee (1998). Samples were normally sectioned in one of three ways T = vertical section oriented parallel with ice direction [tectonic]; P = vertical section oriented perpendicular to ice direction [perpendicular]; H = horizontal section oriented parallel to ice direction [horizontal]. These were then analysed using a Nikon Eclipse 50i Petrological Microscope under plane and cross-polarised light. The slides were interpreted using a combination of the descriptions by van der Meer (1993), Menzies (2000) and Hart et al. (2004).

The microstructures seen were defined as follows: *skelsepic plasmic fabric* – plasma (clay minerals) displaying parallel orientation to the grain edge; *plaster* - plastering of plasma (clay minerals) and silt around larger grains; *turbates* – small grains displaying parallel orientation to the edge of a larger grain; *lineations* – lines of clasts; *intraclasts* – lens of different facies; *mini-shear zone* – local highly oriented zones normally formed between large grains.

The VIPS image processing package (Cupitt and Martinez, 1996) was used to semi-automatically collect the orientation (from the sections orientated in the tectonic direction) and a-axis length from 100 clasts (from all thin sections) both on the whole slide at the optical scale and at the microscopic scale (normally at a magnification of 40). To calculate variation in grain size in the samples (sorting), the standard deviation was calculated and expressed as a percentage of the mean (s.d. %).

The Oriana software package was used to examine the orientation data. Rayleigh's Uniformity Test (Fisher, 1993) (Z) was applied which calculates the probability of the null hypothesis that the data are distributed in a uniform manner, where:

$$Z = nr^2 \quad (1)$$

where n is the number of observations and r is the length of the mean vector. The mean vector (combination of the individual vectors) has two properties; its direction and length. The length will range from 0 to 1; a larger r value indicates that the observations are clusted around the mean. A probability (p) less than 0.05

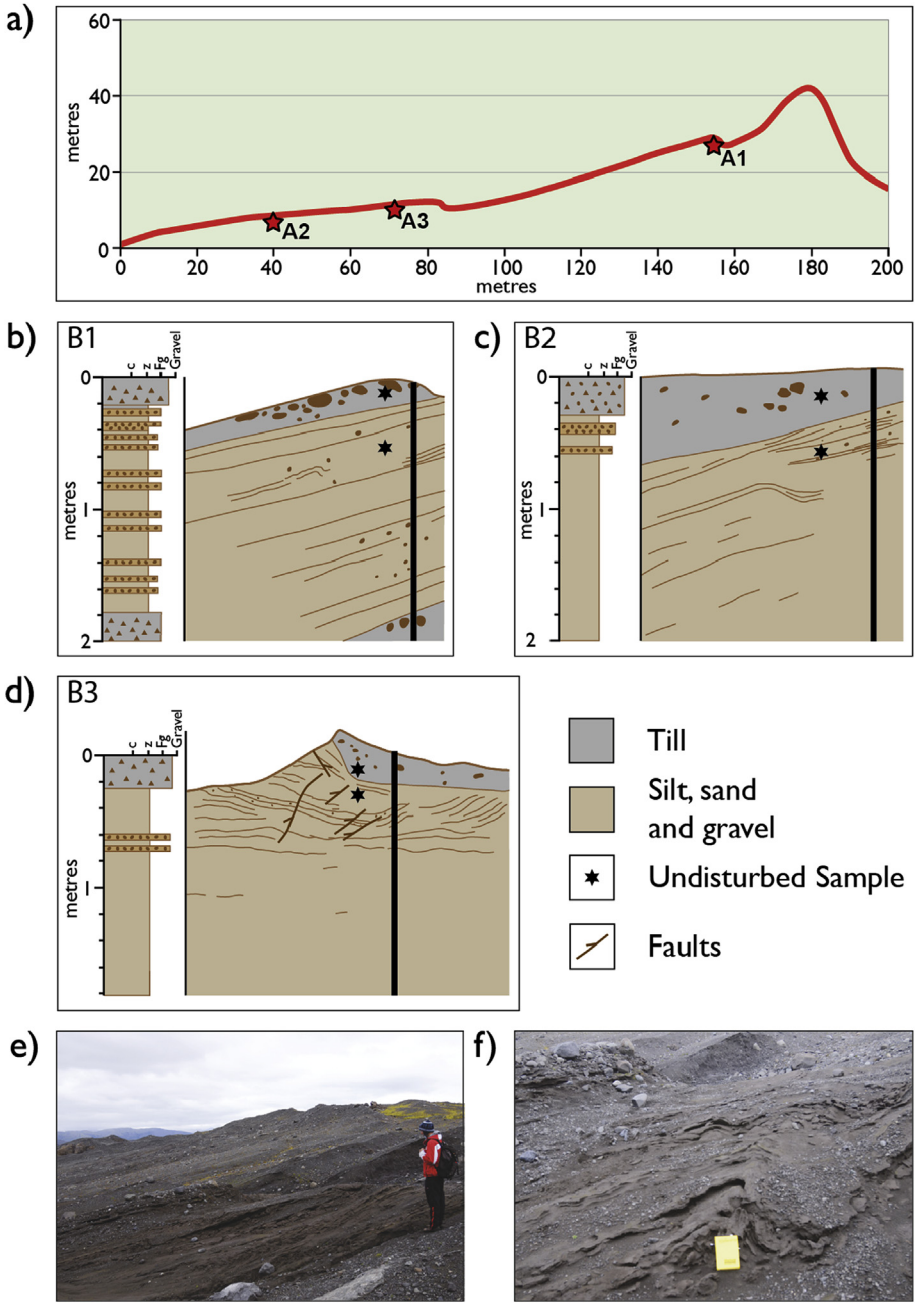

Fig. 3. Details of the moraines at Site B: a) transect across the foreland (see Fig. 1d for location, distance measured as from the 2008 glacier margin) (hill at 180 m marks the 2000 moraine); b),c) and d) section diagrams and facies logs (location indicated by the thick line); e) photograph of moraines at location B1; f) photograph of the recumbent folds observed at location B2. Note: section diagrams b and c are orientated parallel with ice flow, left to right; whereas section diagram d is orientated perpendicular to flow.

indicates that the data were not distributed uniformly and that they show evidence of a preferred direction. The strength of any preferred orientation is reflected by the length of the mean vector.

4. Results

4.1. Grain size

The results of the grain size analysis are shown in Fig. 5 and Table 1. From this is it can be seen that the sediments divide into three main groups: those that are predominately sand (coarse grained debris in the ice from Site A [SK2, SK3, SK4, SK5, SK6, SK7]) and the moraine sediments from Sites A [SK1], B1 [SK16, SK17], B2 [SK18, SK19] and B3 [SK20, SK21]; those that are predominately silt (subglacial borehole sediments [SK10-15]); and those that have a range of grain sizes (reddish brown clay-rich clasts from the debris in the ice from Site A [SK8, SK9], and the reddish brown till, Site B4 [SK22]).

The majority of the sediment was grey in colour, derived from the basalt and ash. The mean matrix (less than 2000 μm) grain size of the ash-rich englacial debris bands was 150 μm. The mean matrix grain size of the upper grey till at Site B was 117 μm, and for the lower silt, sand and gravel unit the mean was similarly 107 μm. However, the latter had a consistently low clay content (0.1%) whilst it was more variable in the till (5.3–0.1%).

The sediment retrieved from the base of the boreholes was

Table 1
Details of the samples collected.

Sample	Site and details	Estimated distance from margin	Collection			Analysis			Mean grain size (μm)	Mean matrix grain size (less than 2000 μm)	% clay
			Bulk sample	Subglacial sampler	Kubiena tin	Grain size	SEM	Thin section			
SK1	A – Proglacial moraine	2 m beyond the margin	✓			✓			55.99	52.58	2.1
SK2	A – Englacial debris band,	75 m from margin	✓			✓			171.1	171.1	0
SK3	A – Debris cone 0.3 m high,	80 m from margin	✓			✓	✓		90.05	90.05	0.1
SK4	A – Englacial debris band,	60 m from margin	✓			✓	✓		290.0	290.0	0.1
SK5	A – Englacial debris band,	55 m from margin	✓			✓			192.7	192.7	0.1
SK6	A – Englacial debris band,	5 m from margin	✓			✓			68.36	68.36	0.2
SK7	A – Englacial debris band,	5 m from margin	✓			✓			150.2	150.2	0.1
SK8	A – Englacial debris band (reddish brown clay-rich clasts)	5 m from margin	✓			✓	✓		7.7	7.7	44.4
SK9	A – Englacial debris band (reddish brown clay-rich clasts)	5 m from margin	✓			✓	✓		18.86	18.86	19.7
SK10	A – Subglacial – borehole 1	110 m from margin		✓		✓			2.5	2.5	40.7
SK11	A – Subglacial – borehole 3	112 m from margin		✓		✓			2.6	2.6	44.1
SK12	A – Subglacial – borehole 4	92 m from margin		✓			✓				
SK13	A – Subglacial – borehole 6	102 m from margin		✓		✓			3.6	3.6	28.2
SK14	A – Subglacial – borehole 8	92 m from margin		✓		✓			12.07	12.07	1.3
SK15	A – Subglacial – borehole 9	95 m from margin		✓		✓			19.06	19.06	1.0
SK16	B1a - Upper grey till layer	25 m from margin	✓		✓	✓	✓	✓	1490.7	73.15	0.3
SK17	B1b - Lower silt, sand & gravel layer	25 m from margin	✓		✓	✓			164.7	143.2	0.1
SK18	B2a - Upper grey till layer	140 m from margin	✓		✓	✓			164.0	159.2	0.1
SK19	B2b - Lower silt, sand & gravel layer	140 m from margin	✓		✓	✓	✓	✓	89.92	89.92	0.1
SK20	B3a - Upper grey till layer	110 m from margin	✓		✓	✓	✓	✓	365.4	119.8	5.3
SK21	B3b - Lower silt, sand & gravel layer	110 m from margin	✓		✓	✓			87.65	87.65	0.1
SK22	B4–Reddish brown till	200 m from margin	✓		✓	✓	✓	✓	463.4	10.34	22.3

predominantly silt (7.9 μm), that was much finer than the proglacial samples. Rose and Hart (2008) have suggested that if there are boulders present on the till surface, this prevents the sampler from penetrating the till. Normally the sampler collects a sample representative of the matrix, but in this case only the finest fraction of the matrix was sampled due to the boulder-rich till surface which were observed in the foreland. Because of this, it is suggested that the proglacial sample SK1 probably represents the matrix grain size for the subglacial till at Site A.

Since it has been suggested that the till at Sites B1-3 were formed during a readvance over the proglacial lake sediments, it is possible that some of this material was a source for the subglacial till (although, this material itself would be a combination of grains from subglacial, englacial and fluvial pathways redeposited within a lake). SK18 (Site B2) had a high matrix grainsize (low clay content), suggesting a higher percentage of proglacial components. The matrix grain-size distribution and overall grain size of SK16 (Site B1) was very similar to that of SK1 (from subglacial material at Site A) but had a very low clay content suggesting some influence from proglacial sediments. SK20 (Site B3) was intermediate between the two in matrix grain size, but had a much higher clay percentage, which suggests it also comprised a relatively low percentage of proglacial components.

The reddish brown till must derive from small outcrops of Tertiary oxidized paleosols and/or tephra layers which are composed of reddish brown clay. It appears that when this material was initially eroded from the bedrock, it remained cohesive probably due to its high clay content. The angular reddish brown clay-rich clasts (average clast a-axis length 1 cm) within the englacial debris-ice had a mean grain size of 13 μm, and the till at Site B4 had a matrix grain size of 10 μm.

4.2. SEM

Fig. 6 shows the results from the surface texture analysis (separated into the grey and reddish brown materials), Fig. 4 shows some examples, and Table 2 gives a summary of the results.

The grey englacial facies are dominated by ash fragments (vesicles). These have either an irregular (Fig. 4a) or linear shape (Fig. 4b). They have an angular outline, low relief, high RA, and a high percentage of an original surface. However some grains do show evidence of erosion (Fig. 4c). This shows that some of the ash passes through the glacier system with little change, whilst other ash grains undergo erosion (Fig. 4c).

The grey till has lower percentage angular outline and RA, higher percentage of low relief, with little original surface (Fig. 4d and e). The results are similar to the sample from the laminated silt, sand and gravel unit (SK19) (Fig. 4f). Although the grain size of SK12 was not measured (due to a small sample size), we can assume its grain size was similar to the other subglacial samples (SK10-15) which had a mean grain size of 7.9 μm (range 2.5–19.0 μm). In addition, there was a very strong relationship between mean matrix grain size and mean SEM a-axis length for the grey tills ($r^2 = 0.98$). Since we know the mean SEM a-axis for SK12, if we apply the relationship between derived from the other grey tills, this gives a mean matrix grain size of 22.11 μm, similar to the other measured samples.

The englacial reddish brown clay is composed of many smaller fragments (Fig. 4g) (clay conglomerate), some ash fragments (Fig. 4h) and grains with evidence of erosion by ice (Fig. 4i). The englacial samples have a medium angularity, RA and percentage of low relief, and a high percentage of small conchoidal fracture.

The reddish brown till sample has a medium angular outline, but low RA, low percentage of low relief and a high percentage of small conchoidal fracture (Fig. 4j and k), although some grains showed little evidence for erosion (Fig. 4l).

4.3. Micromorphology

The thin section analysis for each sample was carried out in

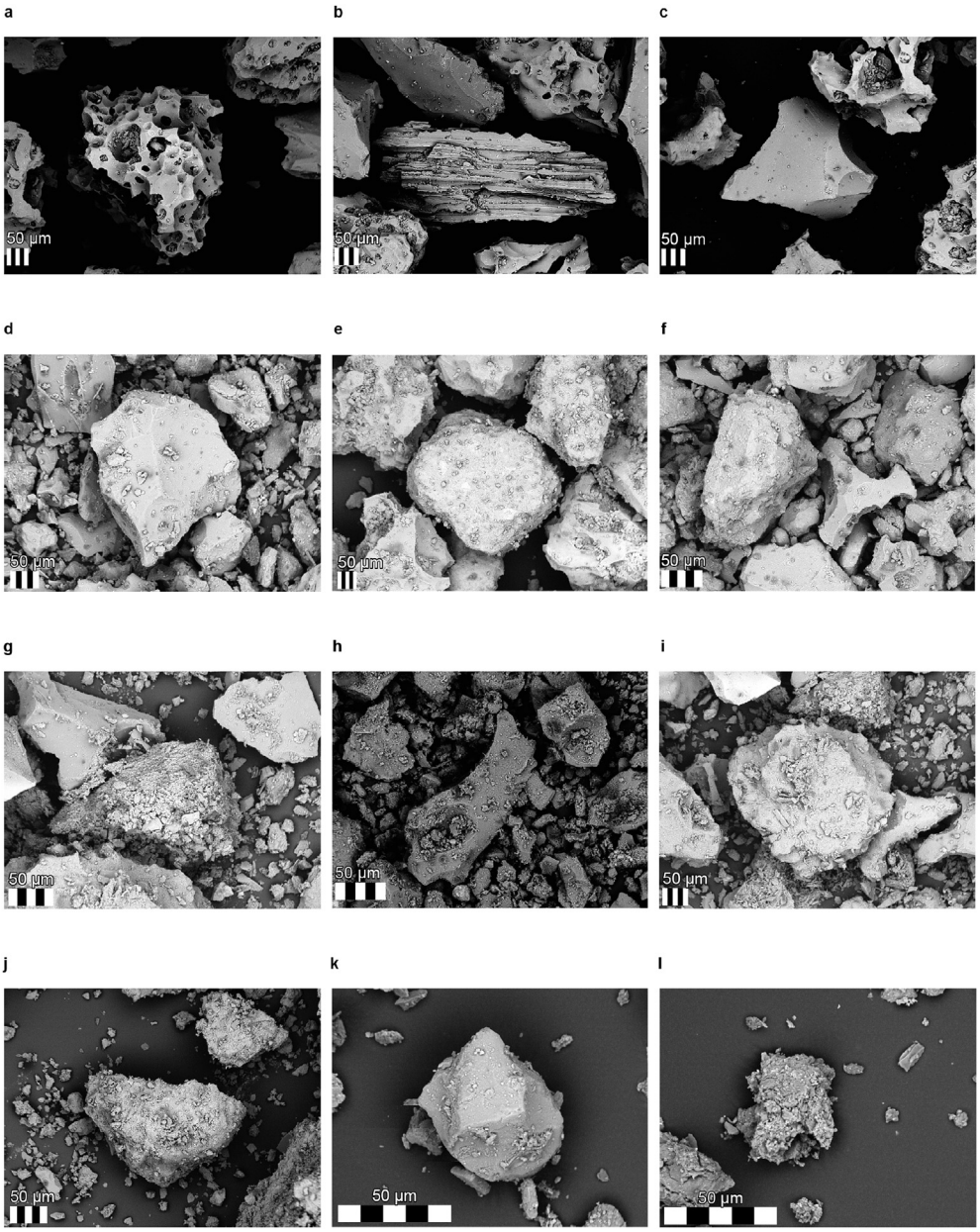

Fig. 4. SEM results: Grey englacial facies (a, b and c), a) irregular ash fragments (SK4/01); b) linear ash fragment (SK4/12); c) grain showing conchoidal fracture; Grey Subglacial Till (d and e), d) grain showing fracture and abrasion (SK16/25); e) fracture dominated by abrasion (SK20/02); Grey Proglacial silts and sand, f) comparison of a round grain (left) and ash fragment (right) (SK21/06); Reddish brown englacial till facies (g,h and i), g) conglomerate clay grain (SK8/25); h) ash fragment (SK9/11); i) rounded grain (SK8/24); Reddish brown subglacial till (j, k and l), j) typical around low relief grain (SK22/01), k) grain showing abrading and fracture (SK22-26), l) original clay conglomerate (SK22/27).

three parts. Firstly the whole slide was examined at the optical scale. Secondly, the slide was examined at microscopic (x 40) scale and an area was chosen at random with no particularly distinguishing features to represent the slide at that scale ('homogeneous'). Finally, specific areas of interest were investigated at x 40 scale. Table 3 shows quantitative data and Table 4 shows the presence or absence of different micromorphological features in the different tills.

4.3.1. Grey till facies

There were two examples of the grey till facies. Sample SK16 (Fig. 7a) has low percentage of clay (0.3%); the thin section as a whole has a fine grain size (691 μm) and low sorting (s.d.% = 69%). In contrast, SK20 (Fig. 7b) has a much higher percentage of clay (5.3%), higher mean grain size (1774.5 μm) with higher sorting (s.d.% = 148%) (Table 3). They also show very different structures when viewed under the microscope (Table 4).

The clay-poor sample SK16 has a statistically orientated microfabric at both the optical and microscopic scale. The microstructures include turbates and lineations (Fig. 8) and mini-shear zones. In addition the till comprises irregular patches of fine grained and coarse grained facies. Two detailed studies were made of the two facies. Both examples have a similar size range, and both facies were well sorted. In both examples the fine-grained facies had an isotropic microfabric, but the coarse-grained facies was oriented in one example and isotropic in the other. In places it appeared that there may be a finer-grained till surrounding the clasts (a possible plaster, discussed in more detail below). However,

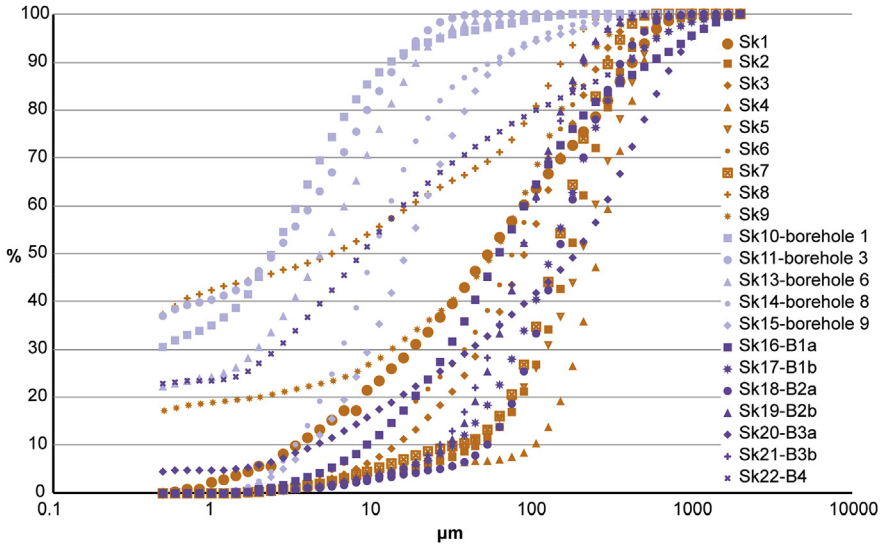

Fig. 5. Grain size analysis results. Orange (SK1-9): sampled adjacent to or on the glacier at Site A. Lilac (SK10-15): subglacial samples sampled from Site A. Purple (SK16-22): Outcrop from Site B. (For interpretation of the references to colour in this figure legend, the reader is referred to the web version of this article.)

a detailed study showed that there was no significant difference in grain size or sorting. The grains surrounding the clasts were not oriented, and the possible plaster carapace was discontinuous.

It is suggested that the coarse grained facies derives from the underlying proglacial sediments since at Site B1, the matrix of the till (SK16) is much finer than the proglacial sediments (SK17) (Table 1).

The microfabric of the clay-rich sample SK20 was also anisotropic at both scales. The microstructures include plaster and turbates (Fig. 9a), and distinctive intraclasts of till. These are mostly rounded or semi-rounded with some angular intraclasts (Table 3) (Fig. 9b). In places these intraclasts form a line (Fig. 9c) and some are deformed (Fig. 9d). Observation along the edges of some of the intraclasts shows penetration of the intraclast facies into the main till body (Fig. 9e). Fig. 9f shows how some parts of the till comprise a darker facies similar to that found in the intraclasts.

The intraclast facies (as in the feature shown in Fig. 9c) was coarser than the normal till matrix, but the particles were not oriented. However, the particles in the matrix in this location were also not well oriented. The intraclast-like facies shown in Fig. 9f had a similar grain size to the matrix, and was oriented. The plaster around the clast shown in Fig. 9a was also examined. The grain size was very fine with an oriented fabric.

There is not such an obvious link between the different facies and the underlying proglacial sands in this sample. The proglacial sediments (SK21) at Site B3 were finer grained than the till (SK20) (Table 1) and it is suggested that the lighter facies may relate to the proglacial sediments, however it was not always the finest grained facies.

4.3.2. Reddish brown till facies

The reddish brown till (SK22) has a high percentage of clay (22.2%); although the thin section as a whole has a coarse grain size (1401 µm) and high sorting (122%). The sample has a statistically orientated microfabric at the optical scale, but not at the microscopic scale. The microstructures include a variety of turbates, including 'normal' turbates (flow around a grain), but also 'matrix' turbates with no central core as well as turbates around till intraclasts (Fig. 10a, b and c). Fig. 10d shows an example of a shear zone between two larger clasts. This is relatively coarse grained, poorly sorted and anisotropic.

A distinctive aspect of the reddish brown till is the different styles of plaster and intraclast. Fig. 11a shows a typical plaster around a clast. Here the grains within the plaster are anisotropic, fine-grained and well sorted. The grains within the surrounding matrix are isotropic and those in the adjacent clay-rich (black) facies was anisotropic. Fig. 11c shows a till intraclast. Fig. 11b show a dark ring of fine grained material (plaster) surrounding a till intraclast. The microfabric of the intraclast till of the latter was investigated; this was fine grained, and isotropic.

Within the till there are intraclasts of clay, and a typical example is shown in Fig. 12. These are assumed to be derived from the clay-rich bedrock. This comprises a relatively undeformed core, with a more deformed carapace often including small till intraclasts. The overall form of this clay intraclast is normally attenuated. Some detailed microfabric studies were made of two till intraclasts within a larger clay intraclast. They were both fine grained, well sorted and isotropic. Examples of the deformation of the clay and till are shown in Fig. 13.

5. Interpretation

Firstly, a comparison is made between the englacial debris and the subglacial till based on the SEM and grain size analysis results. This is followed by a study of the subglacial processes from the thin section analysis.

5.1. A comparison of the erosion in the debris and subglacial till

Numerous researchers have argued that features typical of subglacial erosion include arcuate steps, crescentic gouges, large breakage blocks, fractures plates and subparallel linear fractures (Margolis and Kennet, 1971; Krinsley and Doornkamp, 1973; Krinsley, 1980; Mahaney et al., 1996). These features are clearly seen within the samples (Fig. 6, summary in Table 2).

Soft bed subglacial comminution (grain erosion) can occur either by abrasion or fracture within the deforming layer (Hart, 2007). A number of researchers have argued from laboratory and mathematical experiments, that a force network, represented by force-chains, transmits stress during deformation (Hooke and Iverson, 1995; Jaeger et al., 1996; Iverson et al., 1996; Peters et al., 2005; Damsgaard et al., 2013). Voivret et al. (2009) demonstrate

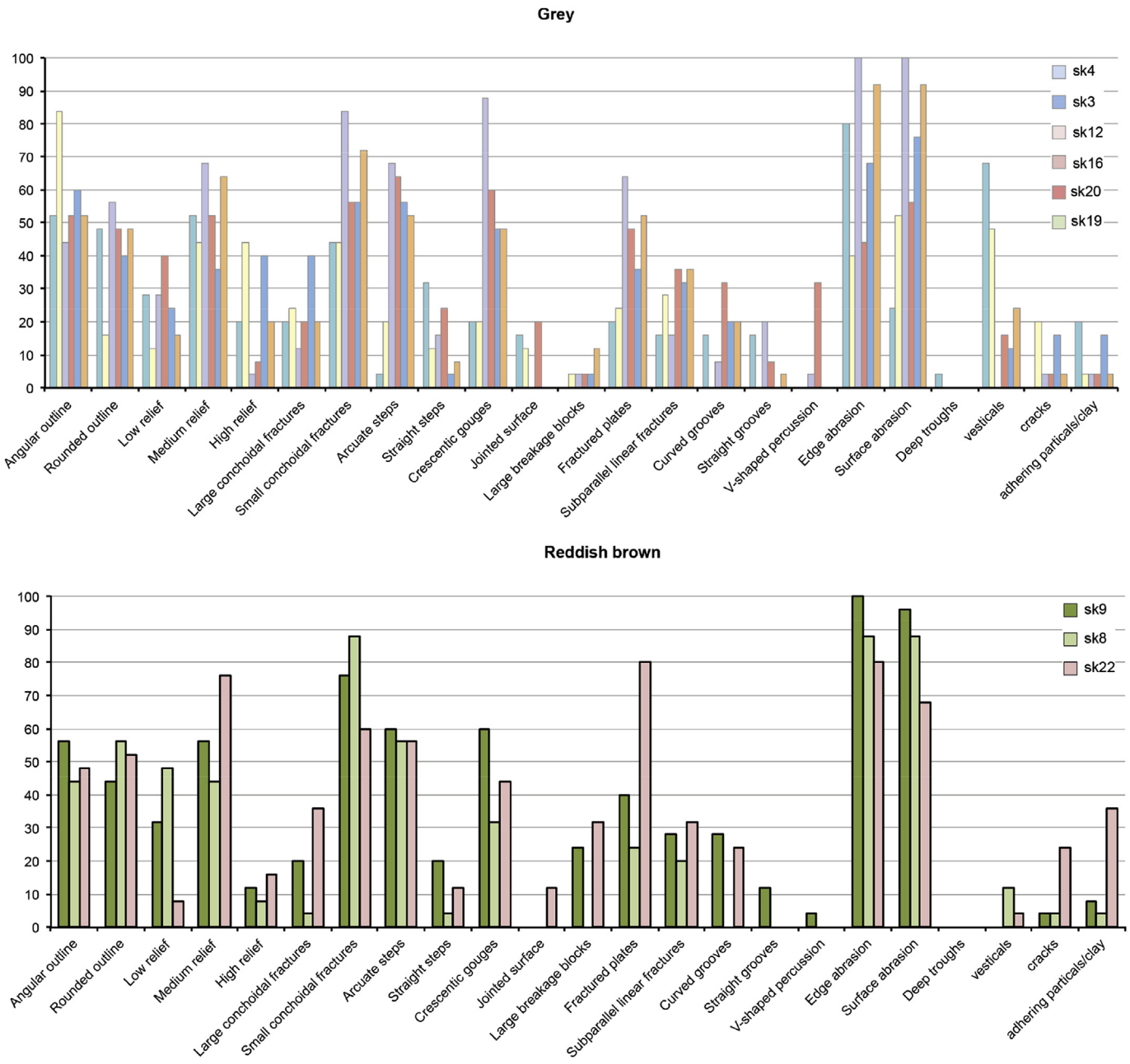

Fig. 6. Results from SEM surface texture analysis from the grey (upper graph) and reddish brown (lower graph) tills.

how stresses often concentrate in large grains, with some (usually smaller) particles excluded from the force-chain network and so are unaffected. Damsgaard et al. (2013) suggest that the failure of force-chains can be caused by particle crushing, rotation, sliding or changes in the stress field due to changes in pore-water pressure.

Those grains excluded from the force-chain network may retain their original surface (as seen at Skálafellsjökull). Fracture may occur due to particle failure in a force-chain (Hooke and Iverson, 1995; Ouchiyama et al., 2005), these may have a highly conchoidal form (e.g. Fig. 4c and d). In addition, particles that have been sheared against smaller grains will be dominated by abrasion and develop a rounded form (e.g. Fig. 4e and f (left), i and j). These may be the result of the larger particles being cushioned by smaller particles (after breakup of the particles from stress fracture), or the reorganisation of the material as a result of dilation. Within a complex deforming layer, grains will be affected by both processes, although one will probably be more dominant (e.g. Fig. 4d and k) (Hart, 2006b).

It has also been suggested that the erosion of grains leads to a terminal grain size (Dreimanis and Vagners, 1971; Haldersen, 1981; Sharp and Gomez, 1986; Iverson et al., 1996). Hooke and Iverson (1995) argued that the final grain-size distribution will be fractal as this arrangement is optimal for distributing internal stresses and minimizing stress heterogeneities. However this model was questioned by Khatwa et al. (1999) who showed that fractal dimensions of supraglacial and subglacial diamicton matrix facies were not significantly different.

We can use the percentage of original surface as a proxy for the length of time and/or amount of erosion (strain history) that the material has undergone. There was a clear difference between SK4

Table 2
Details of the SEM results.

Sample	Facies	Average a-axis (μm)	% low relief	%v-shaped percussion cracks	% small conchoidal fracture	% arcuate steps	% crescentric gouges	% fractured plates	Average % cover of original surface	RA
SK3	Grey englacial debris	178	12	0	44	20	20	24	38	68
SK4	Grey englacial debris	548	28	0	44	4	20	20	70	60
Mean grey debris		*363*	*20*	*0*	*44*	*12*	*20*	*22*	*54*	*64*
SK8	Reddish brown englacial debris	91	48	0	88	56	32	24	8	50
SK9	Reddish brown englacial debris	133	32	24	76	60	60	40	3	48
Mean Reddish brown debris		*112*	*40*	*12*	*82*	*58*	*46*	*32*	*5*	*49*
SK12	Grey subglacial till	26	28	4	84	68	88	64	5	26
SK16	Grey subglacial till	99	40	4	56	64	60	48	3	58
SK20	Grey subglacial till	218	24	4	14	56	48	36	10	46
Mean grey		*114*	*31*	*4*	*65*	*63*	*65*	*49*	*6*	*43*
SK22	Reddish brown subglacial till	274	8	32	60	56	44	80	16	36
SK19	Grey silt, sand & gravel	175	52	12	72	52	48	52	8	48

Table 3
Microfabric and grain size details from Site B.

Sample	Facies	Details	Mean length of vector (r)	Statistically significant if Rayleigh test (p) < 0.05	Mean grain size (μm)	Sorting (SD% mean)
SK16	Grey till	Whole slide (RA = 6)	0.284	✓	690.7	69
		Homogeneous	0.209	✓	71.0	69
		1-Fine grained facies	0.095	x	51.15	33
		1-Coarse grained facies	0.211	✓	132.2	50
		2-Fine grained facies	0.139	x	46.3	69
		2-Coarse grained facies	0.135	x	142.79	58
		Area adjacent to clast	0.104	x	24.63	40
		matrix	0.139	x	39.43	46
SK20	Grey till	Whole slide (RA = 11)	0.284	✓	1774.3	147
		Homogeneous	0.241	✓	87.94	147
		1-Till intraclast (dark facies)	0.164	x	206.8	117
		1-Adjacent matrix (light facies)	0.108	x	123.4	56
		2-Till intraclast-like facies (dark facies)	0.218	✓	121.7	100
		2-Adjacent matrix (light facies)	0.177	✓	130.9	76
		Plaster	0.342	✓	43.0	78
		Adjacent matrix	0.148	x	126.49	151
		Intraclast roundness: (r = 20%, sr = 60%, sa = 17%,a = 3%)				
SK22	Reddish brown till	Whole slide (RA = 8)	0.25	✓	1401.0	122
		Homogeneous	0.121	x	65.9	103
		Shear zone	0.233	✓	106.6	182
		Plaster	0.277	✓	24.5	71
		Matrix	0.127	x	51.4	157
		Black facies	0.186	✓	157.2	105
		Till intraclast/erosional plaster	0.329	x	24.4	115
		1-Till intraclast within a clay intraclast	0.137	x	10.51	45
		2-Till intraclast within a clay intraclast	0.103	x	21.41	69
		Intraclast roundness: (wr = 25%,r = 42%,sr = 33%)				

Table 4
Micromorphological results.

Site	Lithofacies	Micromorphological features								
		Plaster	Skelsepic plasmic fabric and turbates	Till intraclasts	Clay intraclasts	Deformed intarclasts (boudinage)	Intraclast breakdown	Intraclast lineations	Clast lineations	Mini-shear zones
SK16	Grey till		✓						✓	✓
SK20	Grey till	✓	✓	✓		✓	✓	✓		✓
SK22	Reddish brown till	✓	✓	✓	✓	✓	✓			✓

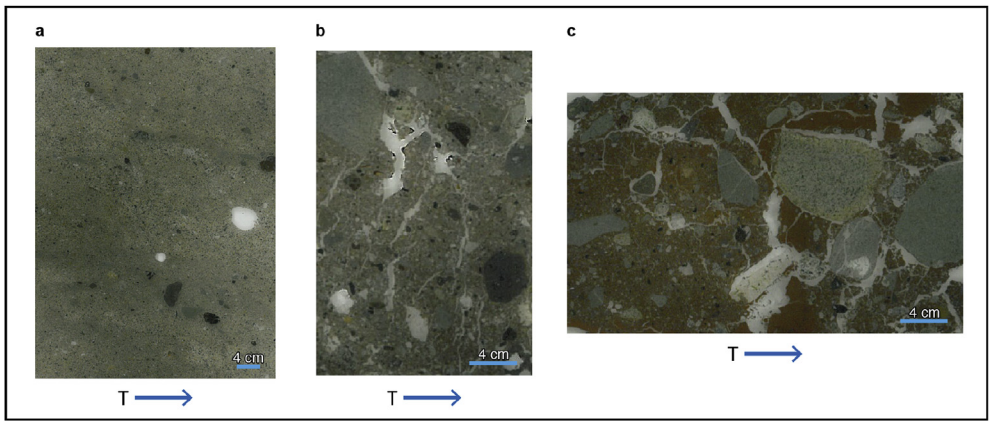

Fig. 7. Thin sections from Skálafellsjökull, Site B: a) SK16, b) SK20, c) SK22. Arrows mark the tectonic direction.

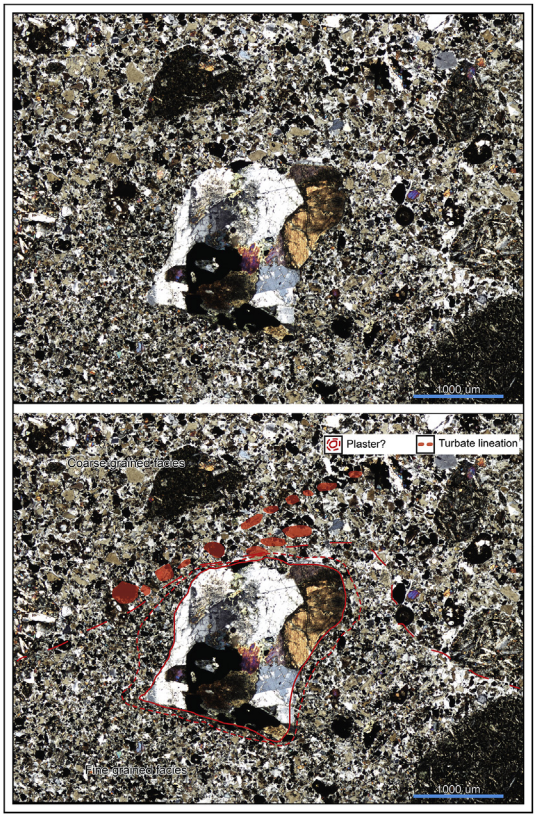

Fig. 8. Micromorphological details of the clay-poor grey till SK16 showing turbate, lineation, possible plaster, fine and coarse grained facies.

(englacial debris) (70% original surface), SK3 (englacial debris) (38% original surface) and SK12 (subglacial till) (5% original surface) (grey lithology without the effects of proglacial incorporation), and a corresponding reduction in grain size and decrease in RA. Material derived from the local geology would have been transported through the glacial system, and have experienced different amounts of erosion. Englacial material will be derived from a variety of sources (both supraglacial and subglacial). We would argue sample SK4 comprises a material that has undergone the least erosion, and has a high component of supraglacial debris. In contrast, SK3 has undergone intermediate levels of erosion, and reflects grains with a more complex transport history (higher subglacial component). The grains in the subglacial till (SK12) have undergone the most erosion.

The subglacial tills that have a proglacial input (SK16 and SK20) similarly have a low percentage original surface, lower grain size and RA (than the englacial debris). This reflects direct subglacial erosion as well as the incorporation of proglacial sediments, which have very similar characteristics as they were derived from subglacial tills.

The percentage of original surface is not a good measure of overall erosion in the reddish brown lithology due to the clay structure. Instead the percentage of fracture plates (low in the debris, 32% SK8 and 9; high in the till, 80% SK22) and roundness (angular in the debris, RA 49%; rounded in the till, RA 36) indicate the change from debris to till.

We suggest this allows us to investigate the evolution from debris to till. Allowing for the complexities discussed above, our results show the reduction in grain size from englacial debris to till for the grey lithology was at least 21% and for the reddish-brown lithology was at least 13%. In addition, the overall rounding of the grains (RA) from the debris to the till was at least 32% for the grey lithology and 26% for the reddish-brown lithology.

In order to attempt to quantify the relative amounts of abrasion and percussion in the debris and tills we have used the textural characteristics results. The percentage of grains with low relief is a good indicator of abrasion (at the scale of grain studied - see Table 2), and the percentage of crescentic gouges is a good indicator of percussion. Using these indices we can investigate both amount, and styles of erosion for the grey lithology (Fig. 14) as a function of shear strain. There is an erosional style continuum from the debris (SK3 & 4—low shear strain) to the tills (high shear strain). It could be argued that percussion would be more efficient at low strains where the grain-size distribution is narrower and as the material approaches the fractal grain-size distribution, abrasion dominates. These indicators may reflect the crystallographic structure of the mineral, may not have universal application. This relationship does not really apply to reddish-brown till, probably due to the high clay content (discussed in more detail in section 5.7).

5.2. Deformation of the subglacial till

The structures described in Table 4 can be divided into rotational features (plaster, skelseptic fabric and turbates) and linear features (lineations, shears, boudinage and mini-shear zones [localised shear zones associated with larger grains]) (Hart, 2006b). Numerous researchers have argued these structures are typical of subglacial deformation (van der Meer, 1997; Khatwa and Tulaczyk,

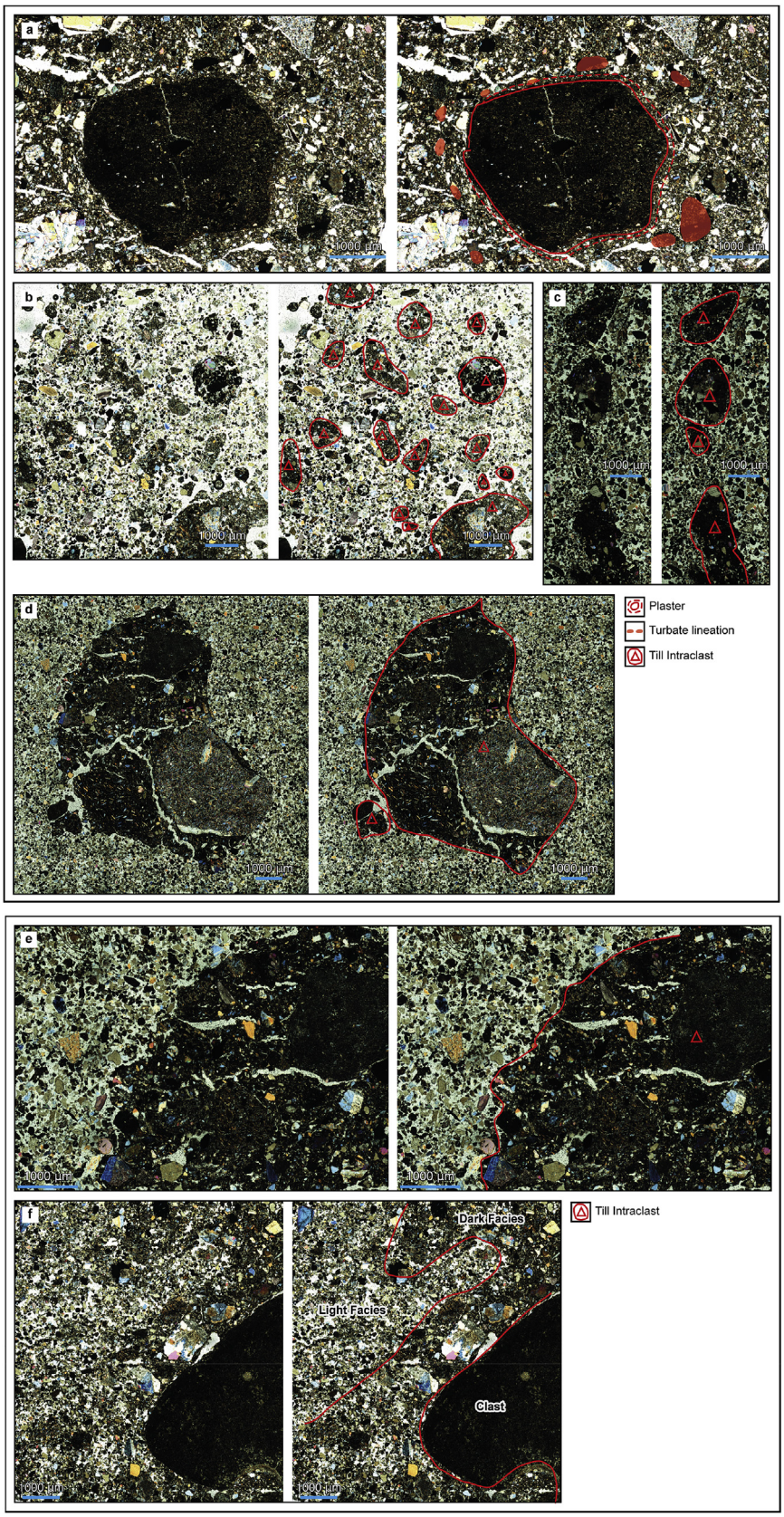

Fig. 9. a. Micromorphological details of the clay-rich grey till SK20: a) showing turbates and plaster; b) Rounded till intraclasts; c) intraclast lineation; d) deformed intraclast. b. Micromorphological details of the clay-rich grey till SK20: e) detail of the deformed intraclast (shown in d); f) dark facies (top right) similar to intraclast facies.

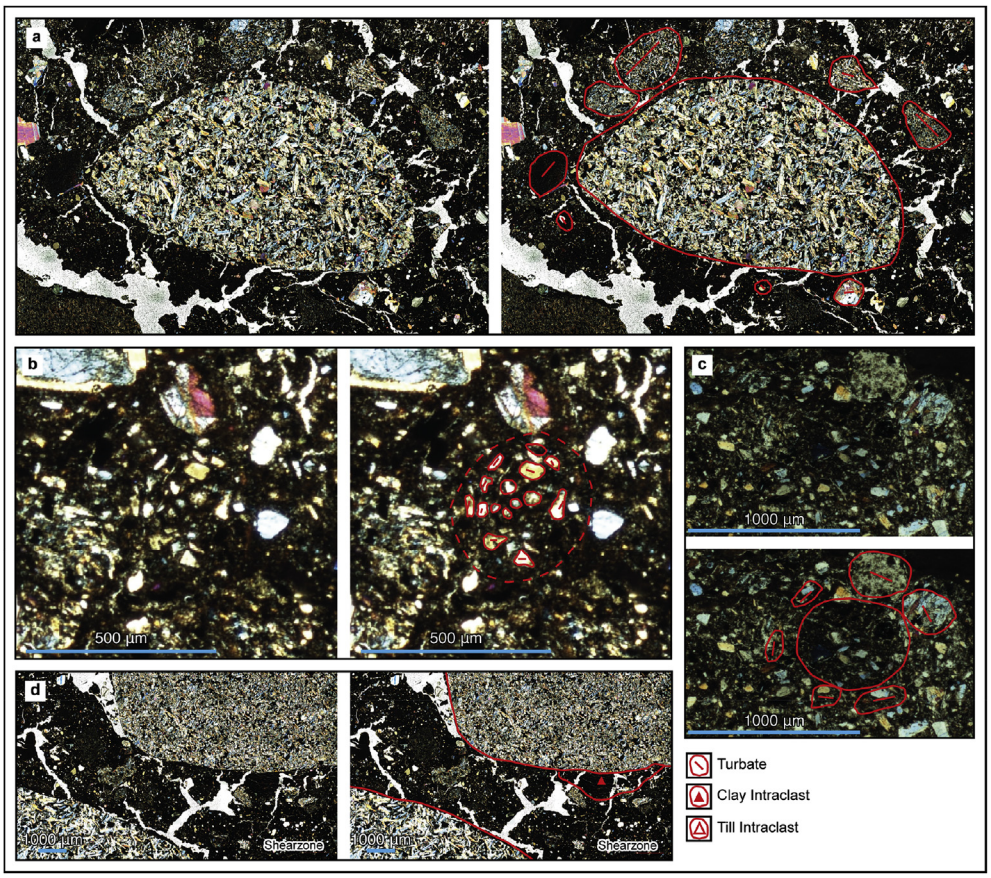

Fig. 10. Micromorphological details of the reddish brown till SK22: a) showing turbates; b) matrix turbates; c) turbate around till intraclast; d) shear zone between two clasts (plus detail of clay intraclast).

2001; Carr and Rose, 2003; Hiemstra and Rijsdijk, 2003; van der Meer et al., 2003; Hart et al., 2004; Menzies et al., 2006; Menzies, 2012; Reinardy et al., 2011; Menzies et al., 2016), and form as a result of simple shear within a subglacial deforming layer (Hart et al., 1990; Roberts and Hart, 2005). This produces rotation, extension and compression (Means, 1976; Hart and Boulton, 1991) which causes the erosion/breakdown and deformation of material (Fig. 15a), and the formation of individual structures are discussed in more detail below.

5.3. Intraclasts

Till intraclasts typically form where there are distinct till facies, which are effected by folding, shearing, attenuation and boudinage (Fig. 15b). Once they are formed within a shear zone, they act as obstacles within the deforming layer. They will become rounded by rotation, elongated due to longitudinal shear, or folded when effected by a more complex shear/competency regime. The irregular zones of coarser material observed in the clay-poor grey till (SK16) (Fig. 8) may result from incorporation and then attenuation of the proglacial materials from below the till. Similarly this occurred in the clay-rich grey till (SK20) (Fig. 9), along the edge of the intraclast, the till is folded and attenuated on the smaller scale, and in this way the intraclasts will become broken down to form a darker facies (Fig. 9e).

5.4. Clay erosion/breakdown

A similar pattern of deformation was seen in the clay in the reddish brown till (Fig. 15b). Once the clay undergoes subglacial shear (by rotation and attenuation) it begins to break down and 'mix' with the till. Since clay is highly cohesive it will have a different competence from the till. In some locations, the till appears to be the more competent material (Fig. 13a, b and c), whilst in others it is the clay (Fig. 13 d, e and f).

Initially, during the subglacial deformation of a clay-rich bedrock, the clay would dominate but overtime it becomes broken down within the till matrix. Given the structures observed it is suggested that attenuation leads to boudinage (Fig. 13b and e; Fig. 15bii), compression results in the brittle faulting (Fig. 13c and f, Fig. 15biii), and rotation causes the intraclast to become abraded/rounded (Fig. 13a and d, Fig. 15bi).

5.5. Plaster

It has been argued (van der Meer, 1993; Hart, 2007) that there were two forms of plaster. A depositional type, where fine grained material is accreted on to the grain as it rotates (Fig. 15ci), and an erosional form where an intraclast is eroded into a smaller form by rotation until only a carapace remains (Fig. 15cii). This was clearly seen within the reddish brown till at Skálafellsjökull. Fig. 11a and b shows a depositional form (plasters around a clast or intraclast) and Fig. 11c illustrates an erosional form. Once intraclasts of material are produced within the deforming layer, due to boudinage, shearing or folding, they will be deformed (attenuated) and/or rotated within the deforming layer. These intraclasts themselves can form a depositional plaster (Fig. 11b).

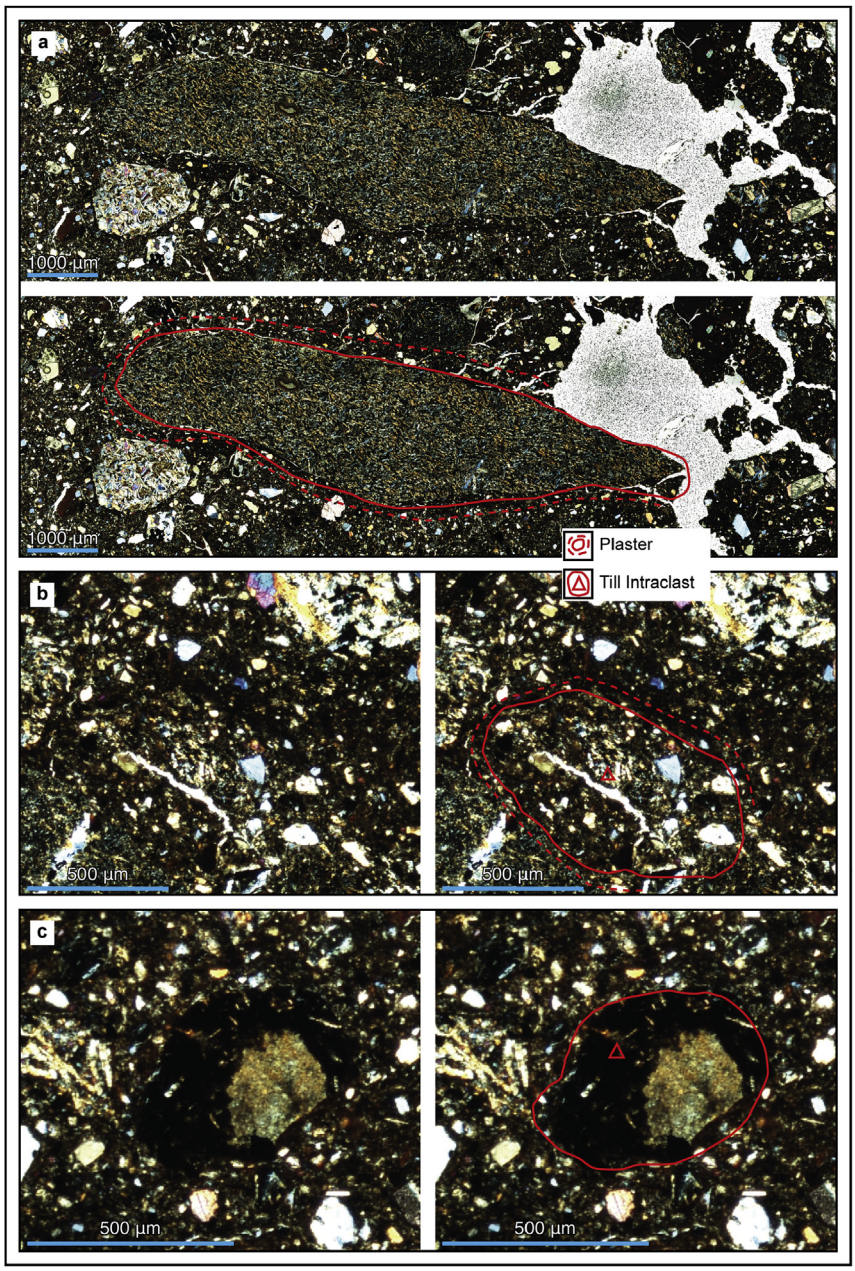

Fig. 11. Micromorphological details of the plaster and till intraclasts in the reddish brown till: a) typical plaster around a clast b) till intraclast surrounded by plaster; c) intraclast of the black till facies.

5.6. Fabric

Field and theoretical studies have shown that fabric within a deforming layer can be either weak or strong (Jeffrey, 1922; March 1932; Glen et al., 1957; Thomason and Iverson, 2006; Hart et al., 2009; Damsgaard et al., 2013). The factors promoting continuous particle rotation (weak fabric) are simple shear, interaction between inclusions and a higher inclusion concentration (Ghosh and Ramberg, 1976; Hart, 1994; Hicock et al., 1996; Mandal et al., 2005; Evans et al., 2016). Factors promoting clasts behaving as a passive strain marker (strong fabric) would be a thin shear zone (Hart, 1994; Benn, 1995), inclusion/matrix slippage (Ildefonse and Mancktelow, 1993; Iverson et al., 2008), pure strain, elongation of inclusions and pre-existing matrix isotropy (Ceriani et al., 2003; Kjaer and Kruger, 1998; Carr and Goddard, 2007). Thomason and Iverson (2006) were able to simulate these stable conditions in ring-shear experiments, and show how increased strain, lead to an increase in anisotropy. However, in the subglacial shear zones conditions (e.g. grain-size, sorting, pore-water pressure, shear zone thickness) are always changing and so the relationship between strain and fabric is more complex.

There was no relationship between mean grain size and strength of orientation (length of mean vector r) for the samples at the optical scale. At the microscopic scale there was a general positive trend (Fig. 16a). There was also a relationship between increased clay content and decreased microfabric strength at both the optical and microscopic scale ($r^2 = 0.95$ and $r^2 = 0.79$ respectively) (Fig. 16b). The fabric strength of the tills within the intraclasts were indistinguishable from the matrix, but the results from the plaster are distinctly fine grained and highly oriented. However,

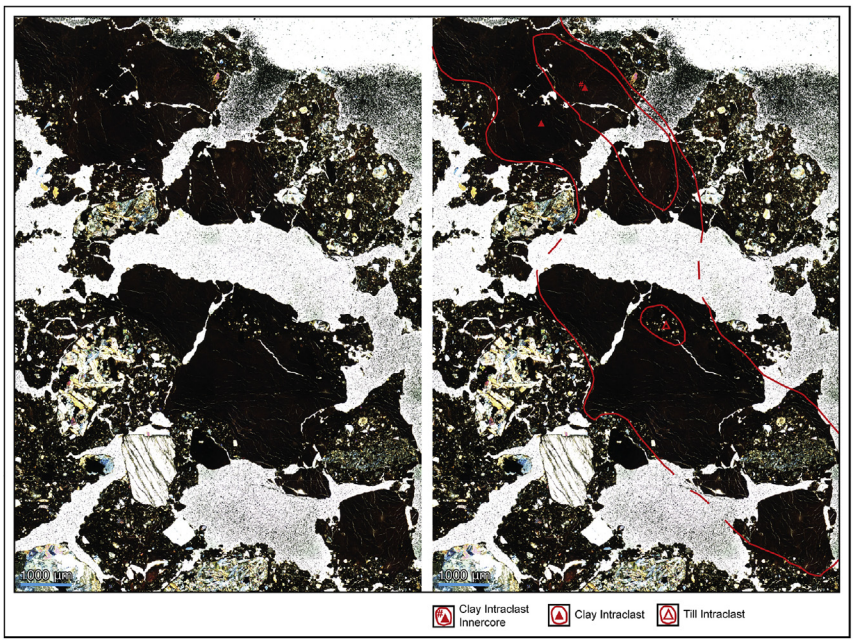

Fig. 12. A typical example of a clay intraclasts in the reddish brown till, showing an inner core, and outer deformed carapace with till intraclasts.

there was no relationship between sorting and fabric strength, which has been previously, reported in the literature (Hart et al, 2004; Hart, 2007).

5.7. Deformational style

The two grey tills (SK16 and 20) have a higher mean grain size (Table 1), higher percentage of grains with low relief, lower percent original cover and higher RA values (Table 2), than the reddish brown till (SK22). The clay-rich grey till (SK20) is intermediate (between SK16 and SK22) in all these parameters (apart from grain size).

The two grey tills have some similarities in deformational style and microfabric, and both comprise two till facies (coarse and fine grained). The clay-rich SK20 contains a series of intraclasts (which are more poorly sorted than the matrix), whilst clay-poor SK16 contains irregular bodies of fine and coarse grains facies.

Overall the grey till was dominated by lineations and boudinage with an anisotropic microfabric. This reflects a longitudinal shearing dominance. In contrast, the reddish brown till was dominated by turbates and plaster with an isotropic microfabric, reflecting a rotational dominance.

A number of researchers have attempted to reconstruct strain from within the deforming layer from ring shear experiments (Larsen et al., 2006; Thomason and Iverson, 2006) and thin section analysis (Hiemstra and Rijsdijk, 2003; Menzies et al., 2016). Larsen et al. (2006) suggested that as shear strain was increased (within a ring-shear experiment), the number of microstructures increased until strain reached a threshold (strains between 7 and 18). After this the number of structures did not increase, and the types of structures remained similar at different strains.

In contrast, Menzies et al. (2016) have argued that increasing strain and/or time lead to distinctive microstructures, from the development of edge-to-edge grain crushing through grain stacks (lineations), microshears, rotational structures, deformation bands/shear zones (mini-shear zones) to domains (intraclasts).

Our results do not agree with this latter model. Instead we suggest that our results are closer to the ring shear experiments of Larsen et al. (2006) and reflect a deformation cycle (Hart, 2007). Materials of different competence within the deforming layer are subjected to simple shear which is affected by both compression and extension leading to a predominance of rotation or attenuation. Neither one necessarily represents more strain than the other. New material is constantly being brought into the deforming layer (from the ice above, advection from the deforming layer up glacier, and incorporation from the underlying layer, Hart and Boulton, 1991), so microscale deformation patterns are always changing.

Menzies et al. (2016) suggest that grain-size (in particular, clay content) will affect their deformation continuum, based on laboratory studies by Tembe et al. (2010) on clays in fault gauges. Although, the clay contents for the microstructure regimes from these experiments (Skempton, 1964; Lupini et al., 1981; Logan and Rauenzahn, 1987; discussed in Tembe et al., 2010) are much higher than found in normal tills, they do show similar structures to till studies. Tembe et al. (2010) describe three regimes and the associated deformation features: regime A (high strength), 0–25% clay with lineations and shears; regime B (intermediate strength), 25–70% where quartz grains are relatively well preserved and surrounded by clay, with shears; and regime C (high strength), over 70% clay with pervasive alignment of clay grains, discontinuous alignment of sand grains, and little quartz grain fracturing.

Our results, although all within the lower regime, show the following relationship between clay content and deformational pattern. As clay content increases from SK16 (0.3%) to SK22 (22.3%) we see a decrease in both abrasion and percussion, a change from clast lineations (at low clay contents) to intraclasts (both till and clay) and presence of a plaster (at higher clay contents). We also see a decrease in microfabric fabric strength with an increase in clay content at the optical and microscopic scale. The low clay content tills are dominated by longitudinal shearing and the high clay content tills by rotational shearing.

Larsen et al. (2006) report contrasting microstructures from two tills with similar grains-size. The Knud Strand tills (Denmark) (Larsen et al., 2004) had predominately brittle forms and the Kurzetnik till (Poland) (Larsen and Piotrowski, 2003) had predominately ductile forms. Larsen et al. (2006) suggest the different

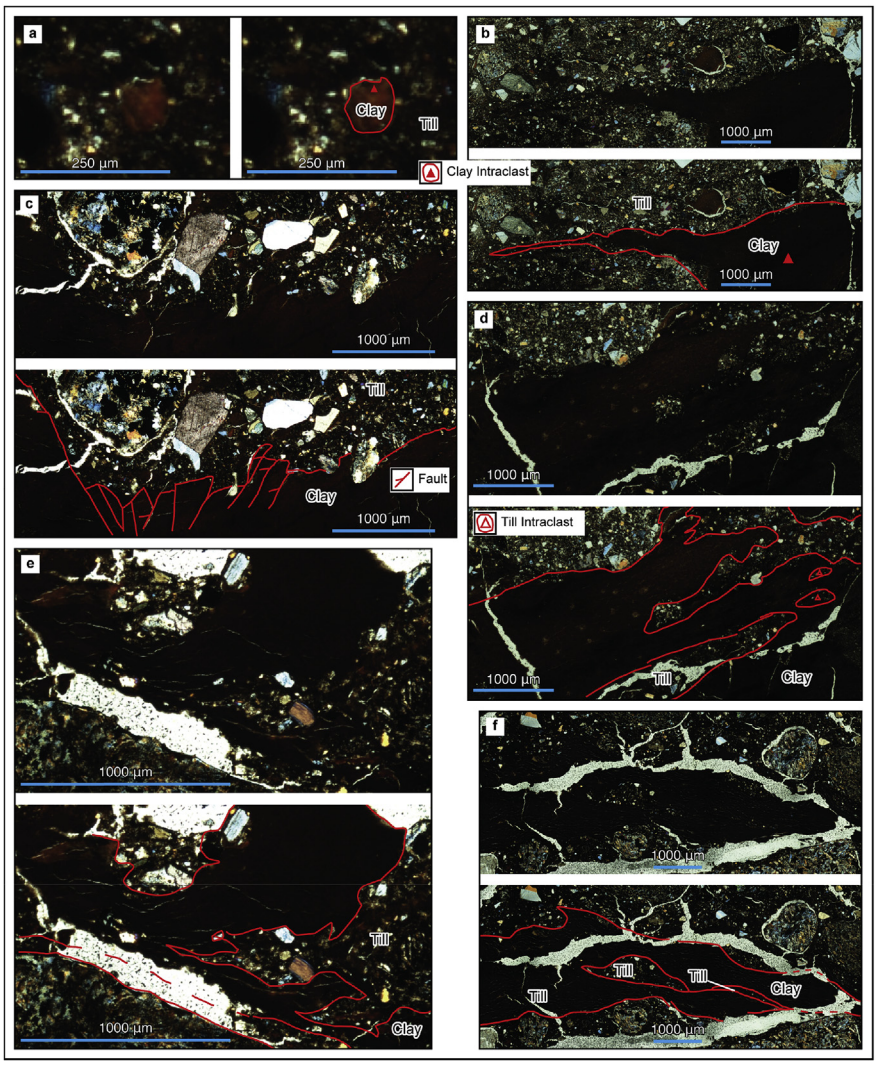

Fig. 13. Micromorphological details of the deformation of clay intraclasts in the reddish brown till: a) small rounded clay intraclast; b) attenuation and boudinage of the clay intraclast; c) clay sheared into till; d) till lenses within a clay intraclast; e) attenuation and boudinage of the till; f) till sheared into clay intraclast.

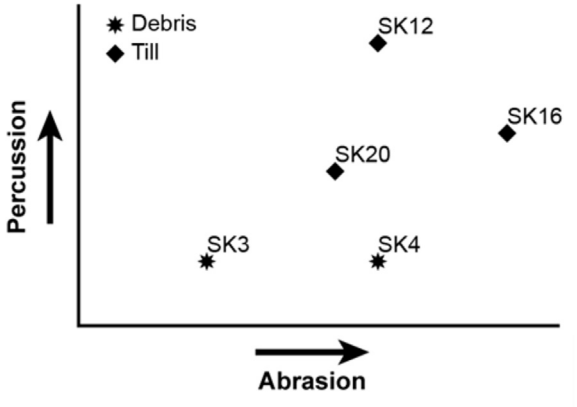

Fig. 14. Erosional style continuum (shown with grey arrow) from debris to subglacial tills (see text for details).

microstructures reflect different deformation histories; with the former resulting from multiple basal decoupling and coupling events (Piotrowski et al., 2006). Similarly, Hart et al. (2011a) suggested brittle deformation would result from winter stick-slip events.

We have data from three subglacial environments: a) grey till overlaying till and bedrock (Site A); b) grey till overlying proglacial sediments (which would be derived from the subglacial and lacustrine environments) (Site B1-3); and c) reddish brown till overlying till and bedrock (Site B4). Although it could be argued that shear stresses will vary within the subglacial till associated with the different ice thicknesses and duration at the different sampling sites, there were sufficient similarities in erosional and deformational styles to allow a comparison with the *in situ* data from Site A.

Data from the Glacsweb probes at Skálafellsjökull showed evidence for stable high pressures and variable water pressure cycles with stick-slip motion (Hart et al., 2015). During stable high water pressures, conditions are more likely to produce a constant erosion of the grains, and development (longitudinal shearing or rotation) of the microstructures. However, where variable water pressures occurred this would lead to changes in the thickness of the deforming layer, leading to more complex microstructure development. Associated with stick-slip motion, there may be periods of bed separation and bed re-connection causing fracture (as

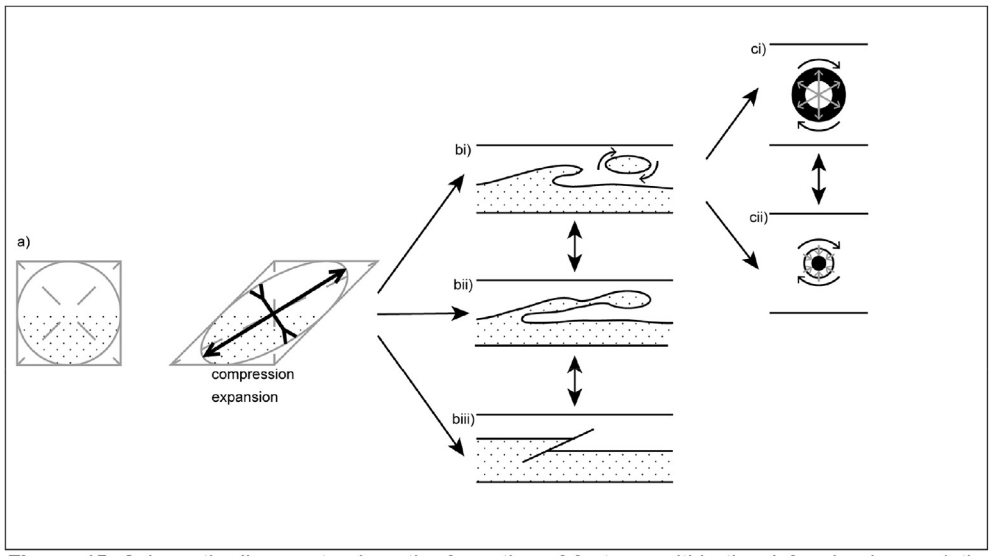

Fig. 15. Schematic diagram to show the formation of features within the deforming layer: a) the effect of simple shear (rotation, extension and compression) on a theoretical two layered unit within a shear zone; b) till or clay intraclasts in a zone, i) dominated by rotation (ductile); ii) dominated by extension (attenuation and boudinage) (ductile); iii) dominated by compression (brittle); c) formation of plaster within the deforming layer (not a scale, these may be grains or intraclasts), i) depositional plaster where fine grained material (shown as black) is accreted on to the grain ii) erosional plaster where an intraclast (shown in white) is 'eroded' into a smaller form.

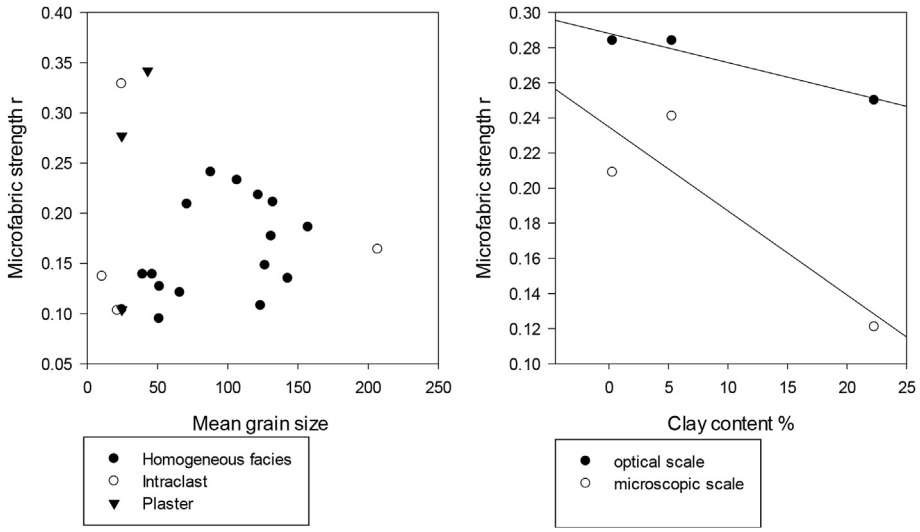

Fig. 16. a) Graphs showing a) mean grain size and b) clay content against microfabric orientation strength (length of mean vector r) for the microscopic scale for the tills (data from Table 3).

suggested by Piotrowski et al., 2006; Hart et al., 2011a).

Thus, the resultant microstructures within a till will be dependent of shear strain, glaciological conditions (deformation history) and grain size and this has been clearly demonstrated at Skálafellsjökull.

6. Conclusion

This is a study of the formation of deformation till beneath a modern Icelandic glacier. We show the evolution from debris into till for two lithofacies. We demonstrate how some grains pass through the glacier system relatively undisturbed, whilst others undergo comminution (grain erosion). Once within the subglacial deforming layer, grains will be sheared, and be dominated by both percussion and abrasion.

Within the till we show the microstructures resulting from the deformation within a subglacial shear zone. This includes linear structures such as lineations, shears, localised shear zones and boudinage; as well as rotational structures including turbates and plaster. In addition there is evidence for intraclasts of both till and clay. These form within a shear zone, and act as obstacles to flow, and become incorporated into the till. We demonstrate the rotational and extensional deformational processes which act together to cause further breakdown (erosion) within the deforming layer.

We are able to demonstrate different processes occur in response to clay content within the till. The tills with low clay content were dominated by longitudinal shearing (high levels of abrasion and percussion, lineations and boudinage with an strong microfabric), whilst those with a higher clay content were dominated by rotation (abrasion and percussion, turbates and plaster

with an weaker microfabric).

These processes produce a deformation till, which has many similarities to those found in Quaternary environments, and so these can be used to help reconstruction past glaciological conditions.

Acknowledgements

The author would like to thank the Glacsweb Iceland 2008/2011 and 2012 teams for help with probe development and data collection; and to Mark Dover in the Cartographic Unit for figure preparation. Thanks also go to Anders Damsgaard and two anonymous reviewers for very constructive reviews, which improved the quality of the manuscript. This research was funded by EPSRC (EP/C511050/1), Leverhulme (F/00 180/AK) and the National Geographic (GEFNE45-12) and the GPR and Leica 1200 GPS units were loaned from the NERC Geophysical Equipment Facility.

References

Alley, R.B., Blankenship, D.D., Bentley, C.R., Rooney, S.T., 1986. Deformation of till beneath ice stream B, West Antarctica. Nature 322, 57–59.
Altuhafi, F.N., Baudet, B.A., Sammonds, P., 2009. On the time-dependent behaviour of glacial sediments: a geotechnical approach. Quat. Sci. Rev. 28 (7), 693–707.
Benn, D.I., 1995. Fabric signature of subglacial till deformation, Breidamerkurjökull, Iceland. Sedimentology 42 (5), 735–747.
Benn, D.I., Ballantyne, C.K., 1993. The description and representation of particle shape. Earth Surf. Process. Landforms 18, 665–672.
Benn, D.I., Evans, D.J., 1996. The interpretation and classification of subglacially-deformed materials. Quat. Sci. Rev. 15, 23–52.
Blake, E.W., Clarke, G.K.C., Gerrin, M.C., 1992. Tools for examining subglacial bed deformation. J. Glaciol. 38, 388–396.
Blott, S.J., Pye, K., 2001. GRADISTAT: a grain size distribution and statistics package for the analysis of unconsolidated sediments. Earth Surf. Process. Landforms 26, 1237–1248.
Blott, S.J., Pye, K., 2006. Particle size distribution analysis of sand-sized particles by laser diffraction: an experimental investigation of instrument sensitivity and the effects of particle shape. Sedimentology 53 (3), 671–685.
Boulton, G.S., Hindmarsh, R.C.A., 1987. Sediment deformation beneath glaciers: rheology and geological consequences. J. Geophys. Res. Solid Earth 92 (B9), 9059–9082.
Boulton, G.S., Jones, A.S., 1979. Stability of temperate ice caps and ice sheets resting on beds of deformable sediment. J. Glaciol. 24, 29–43.
Boulton, G.S., Dobbie, K.E., Zatsepin, S., 2001. Sediment deformation beneath glaciers and its coupling to the subglacial hydraulic system. Quat. Int. 86 (1), 3–28.
Brown, N.E., Hallet, B., Booth, D.B., 1987. Rapid soft bed sliding of the Puget Glacier lobe. J. Geophys. Res. 92.
Carr, S.J., Lee, J.A., 1998. Thin-section production of diamicts: problems and solutions. J. Sediment. Res. 68, 217–221.
Carr, S.J., Rose, J., 2003. Till fabric patterns and significance: particle response to subglacial stress. Quat. Sci. Rev. 22 (14), 1415–1426.
Carr, S.J., Goddard, M.A., 2007. Role of particle size in till fabric characteristics: systematic variation in till fabric from Vestari-Hagafellsjökull, Iceland. Boreas 36 (4), 371–385.
Ceriani, S., Mancktelow, N.S., Pennacchioni, G., 2003. Analogue modelling of the influence of shape and particle/matrix interface lubrication on the rotational behaviour of rigid particles in simple shear. J. Struct. Geol. 25, 2005–2021.
Chandler, B.M.P., Evans, D.J.A., Roberts, D.H., Ewertowski, M., Clayton, A.I., 2016. Glacial geomorphology of the Skálafellsjökull foreland, Iceland: a case study of 'annual' moraines. J. Maps 12 (5), 904–916. http://dx.doi.org/10.1080/17445647.2015.1096216.
Cuffey, K.M., Paterson, W.S.B., 2010. The Physics of Glaciers. Academic Press.
Cupitt, J., Martinez, K., 1996. VIPS: an image processing system for large images. In: Conference Proceedings of the SPIE 1663, pp. 19–28.
Damsgaard, A., Egholm, D.L., Piotrowski, J.A., Tulaczyk, S., Larsen, N.K., Tylmann, K., 2013. Discrete element modeling of subglacial sediment deformation. J. Geophys. Res. Earth Surf. 118 (4), 2230–2242.
Damsgaard, A., Egholm, D.L., Beem, L.H., Tulaczyk, S., Larsen, N.K., Piotrowski, J.A., Siegfried, M.R., 2016. Ice flow dynamics forced by water pressure variations in subglacial granular beds. Geophys. Res. Lett. 43 (23).
Dreimanis, A., Vagners, U.J., 1971. Bimodal distribution of rock and mineral fragments in basal tills. In: Goldthwaite, R.P. (Ed.), Till: a Symposium. Ohio State University Press, Columbus, OH, pp. 237–250. Ohio.
Engelhardt, H., Kamb, B., 1998. Basal sliding of ice stream B, West Antarctica. J. Glaciol. 44 (147), 223–230.
Evans, D.J.A., Twigg, D.R., 2002. The active temperate glacial landsystem: a model based on Breiðamerkurjökull and Fjallsjökull. Icel. Quat. Sci. Rev. 21, 20–22, 2143–2177.
Evans, D.J.A., Phillips, E.R., Hiemstra, J.F., Auton, C.A., 2006. Subglacial till: formation, sedimentary characteristics and classification. Earth-Science Rev. 78 (1), 115–176.
Evans, D.J.A., Roberts, D.H., Evans, S.C., 2016. Multiple subglacial till deposition: a modern exemplar for Quaternary palaeoglaciology. Quat. Sci. Rev. 145, 183–203.
Fischer, U.H., Clarke, G.K., 1997. Stick slip sliding behaviour at the base of a glacier. Ann. Glaciol. 24, 390–396.
Fischer, U.H., Clarke, G.K., 2001. Review of subglacial hydro-mechanical coupling: Trapridge glacier, Yukon Territory, Canada. Quat. Int. 86 (1), 29–43.
Fisher, N.I., 1993. Statistical Analysis of Circular Data. Cambridge University Press, 269pp.
Folk, R.L., Ward, W.C., 1957. Brazos River bar: a study in the significance of grain size parameters. J. Sed. Petrol. 27, 3–26.
Ghosh, S.K., Ramberg, H., 1976. Reorientation of inclusions by combination of pure shear and simple shear. Tectonophysics 34 (1), 1–70.
Gjessing, J., 1965. On 'plastic scouring' and 'subglacial erosion'. Nor. Geogr. Tidsskr. 20, 1–37.
Glen, J.W., Donner, J.J., West, R.G., 1957. On the mechanism by which stones in till become oriented. Am. J. Sci. 255 (3), 194–205.
Haldersen, S., 1981. The enrichment of quartz in tills. In: Evenson, E.B., Schluchter, C., Rabassa, J. (Eds.), Tills and Related Deposits. A.A. Balkema, Rotterdam, pp. 141–150.
Hart, J.K., 1990. Proglacial glaciotectonic deformation and the origin of the cromer ridge push moraine complex, North Norfolk, UK. Boreas 19, 165–180.
Hart, J.K., 1994. Till fabric associated with deformable beds. Earth Surf. Process. Landforms 19 (1), 15–32.
Hart, J.K., 2006a. Athabasca Glacier, Canada—a field example of subglacial ice and till erosion? Earth Surf. Process. Landforms 31 (1), 65–80.
Hart, J.K., 2006b. An investigation of subglacial processes at the microscale from Briksdalsbreen, Norway. Sedimentology 53, 125–146.
Hart, J.K., 2007. An investigation of subglacial shear zone processes from Weybourne, Norfolk, UK. Quat. Sci. Rev. 26, 2354–2374.
Hart, J.K., Boulton, G.S., 1991. The interrelation of glaciotectonic and glaciodepositional processes within the glacial environment. Quat. Sci. Rev. 10 (4), 335–350.
Hart, J.K., Rose, J., 2001. Approaches to the study of glacier bed deformation. Quat. Int. 86 (1), 45–58.
Hart, J.K., Martinez, K., 2006. Environmental Sensor Networks: a revolution in the earth system science? Earth-Science Rev. 78 (3), 177–191.
Hart, J.K., Hindmarsh, R.C., Boulton, G.S., 1990. Styles of subglacial glaciotectonic deformation within the context of the Anglian ice-sheet. Earth Surf. Process. Landforms 15 (3), 227–241.
Hart, J.K., Khatwa, A., Sammonds, P., 2004. The effect of grain texture on the occurrence of microstructural properties in subglacial till. Quat. Sci. Rev. 23, 2501–2512.
Hart, J.K., Martinez, K., Ong, R., Riddoch, A., Rose, K.C., Padhy, P., 2006. A wireless multi-sensor subglacial probe: design and preliminary results. J. Glaciol. 52 (178), 389–397.
Hart, J.K., Rose, K.C., Martinez, K., Ong, R., 2009. Subglacial clast behaviour and its implication for till fabric development: new results derived from wireless subglacial probe experiments. Quat. Sci. Rev. 28 (7), 597–607.
Hart, J.K., Rose, K.C., Martinez, K., 2011a. Subglacial till behaviour derived from in situ wireless multi-sensor subglacial probes: rheology, hydro-mechanical interactions and till formation. Quat. Sci. Rev. 30 (1), 234–247.
Hart, J.K., Rose, K.C., Waller, R.I., Vaughan-Hirsch, D., Martinez, K., 2011b. Assessing the catastrophic break-up of Briksdalsbreen, Norway, associated with rapid climate change. J. Geol. Soc. 168 (3), 673–688.
Hart, J.K., Rose, K.C., Clayton, A., Martinez, K., 2015. Englacial and subglacial water flow at Skálafellsjökull, Iceland derived from ground penetrating radar, in situ Glacsweb probe and borehole water level measurements. Earth Surf. Process. Landforms 40 (15), 2071–2083.
Hicock, S.R., Goff, J.R., Lian, O.B., Little, E.C., 1996. On the interpretation of subglacial till fabric. J. Sediment. Res. 66 (5), 928–934.
Hiemstra, J., Rijsdijk, K., 2003. Observing artificially induced strain: implications for subglacial deformation. J. Quat. Sci. 18 (5), 373–383.
Hindmarsh, R., 1997. Deforming beds: viscous and plastic scales of deformation. Quat. Sci. Rev. 16 (9), 1039–1056.
Hooke, R.L., Iverson, N.R., 1995. Grain-size distribution in deforming subglacial tills: role of grain fracture. Geology 23 (1), 57–60.
Humlum, O., 1985. Genesis of the push moraine at Kötlujökull, Iceland: a commentary. Polarforschung 55 (2), 127–130.
Ildefonse, B., Mancktelow, N.S., 1993. Deformation around rigid particles: the influence of slip at the particle/matrix interface. Tectonophysics 221 (3–4), 345–359.
Iverson, N.R., 2010. Shear resistance and continuity of subglacial till: hydrology rules. J. Glaciol. 56 (200), 1104–1114.
Iverson, N.R., Hooyer, T.S., Hooke, R.LeB., 1996. A laboratory study of sediment deformation: stress heterogeneity and grain-size evolution. Ann. Glaciol. 22, 167–175.
Iverson, N.R., Hooyer, T.S., Baker, R.W., 1998. Ring-shear studies of till deformation: coulomb-plastic behavior and distributed strain in glacier beds. J. Glaciol. 148, 634–642.
Iverson, N.R., Baker, R.W., Hooke, R.LeB., Hanson, B., Jansson, P., 1999. Coupling between a glacier and a soft bed: I. A relation between effective pressure and local shear stress determined from till elasticity. J. Glaciol. 45, 31–40.
Iverson, N.R., Hooyer, T.S., Thomason, J.F., Graesch, M., Shumway, J.R., 2008. The experimental basis for interpreting particle and magnetic fabrics of sheared till.

Earth Surf. Process. Landforms 33, 627–645.
Jaeger, H.M., Nagel, S.R., Behringer, R.P., 1996. Granular solids, liquids, and gases. Rev. Mod. Phys. 68 (4), 1259.
Jeffrey, G.B., 1922. The motion of ellipsoidal particles immersed in a viscous fluid. Proc. R. Soc. 102, 161–179.
Jóhannesson, H., Sæmundsson, K., 1998. Geological Map of Iceland, 1:500 000: Bedrock Geology. Icelandic Institute of Natural History.
Kamb, B., 1991. Rheological nonlinearity and flow instability in the deforming bed mechanism of ice stream motion. J. Geophys. Res. Solid Earth 96 (B10), 16585–16595.
Khatwa, A., Hart, J.K., Payne, A.J., 1999. Grain textural analysis across a range of glacial facies. Ann. Glaciol. 28 (1), 111–117.
Khatwa, A., Tulaczyk, S., 2001. Microstructural interpretations of modern and Pleistocene subglacially deformed sediments: the relative role of parent material and subglacial processes. J. Quat. Sci. 16, 507–517.
Kjaer, K.H., Kruger, J., 1998. Does clast size influence fabric strength? J. Sediment. Res. 68 (5).
Krinsley, D.H., 1980. Scanning electron microscope examination of quartz sand grain micro textures. Kwart. Geol. 24, 217–232.
Krinsley, D.H., Doornkamp, J.C., 1973. Atlas of Quartz Sand Surface Textures. Cambridge University Press, Cambridge, 91 pp.
Krüger, J., 1985. Formation of a push moraine at the margin of Höfdabrekkujökull, South Iceland. Geogr. Ann. 67A, 199–212.
Larsen, N.K., Piotrowski, J.A., 2003. Fabric pattern in a basal till succession and its significance for reconstructing subglacial processes. J. Sediment. Res. 73 (5), 725–734.
Larsen, N.K., Piotrowski, J.A., Kronborg, C., 2004. A multiproxy study of a basal till: a time-transgressive accretion and deformation hypothesis. J. Quat. Sci. 19 (1), 9–21.
Larsen, N.K., Piotrowski, J.A., Christiansen, F., 2006. Microstructures and microshears as proxy for strain in subglacial diamicts: implications for basal till formation. Geology 34 (10), 889–892.
Logan, J.M., Rauenzahn, K.A., 1987. Frictional dependence of gouge mixtures of quartz and montmorillonite on velocity, composition and fabric. Tectonophysics 144, 87–108.
Lupini, J.F., Skinner, A.E., Vaughan, P.R., 1981. The drained residual strength of cohesive soils. Geotechnique 31, 181–213.
Mahaney, W.C., Claridge, G., Campbell, I., 1996. Microtextures on quartz grains in tills from Antarctica. Palaeogeogr. Palaeoclimatol. Palaeoecol. 121, 89–103.
Mahaney, W.C., Kalm, V., 2000. Comparative scanning electron microscopy study of oriented till blocks, glacial grains and Devonian sands in Estonia and Latvia. Boreas 29 (1), 35–51.
Mandal, N., Samanta, S.K., Bhattacharyya, G., Chakraborty, C., 2005. Rotation behaviour of rigid inclusions in multiple association: insights from experimental and theoretical models. J. Struct. Geol. 27 (4), 679–692.
March, A., 1932. Mathematische theorie der regelung nach der Korngestalt bei affiner deformation. Z. für Kristallogr. 81, 285–297.
Margolis, S.V., Kennet, J.P., 1971. Cenozoic paleoglacial history of Antarctica recorded in subantarctic deep-sea cores. Am. J. Sci. 271, 1–36.
Martinez, K., Hart, J.K., 2010. Glaciers monitoring: deploying custom hardware in harsh environments. In: Wireless Sensor Networks - Deployments and Design Frameworks. Springer.
Martinez, K., Hart, J.K., Basford, P., Bragg, G., Ward, T., Young, D.S., 2017. A geophone wireless sensor network for investigating glacier stick-slip motion. Comput. Geosciences 105, 103–112.
Means, W.D., 1976. Stress and Strain. Basic Concepts of Continuum Mechanics for Geologists. Springer-Verlag, New York, 339pp.
van der Meer, J.J.M., 1993. Microscopic evidence of subglacial deformation. Quat. Sci. Rev. 12, 553–587.
van der Meer, J.J.M., 1997. Particle and aggregate mobility in till: microscopic evidence of subglacial processes. Quat. Sci. Rev. 16, 827–831.
van der Meer, J.J., Menzies, J., Rose, J., 2003. Subglacial till: the deforming glacier bed. Quat. Sci. Rev. 22 (15), 1659–1685.
Menzies, J., 2000. Micromorphological analyses of microfabrics and microstructures indicative of deformation processes in glacial sediments. In: Maltman, A.J., Hubbard, B., Hambrey, M.J. (Eds.), Deformation of Glacial Materials, vol 176. Geological Society Special Publication, pp. 245–258.
Menzies, J., 2012. Strain pathways, till internal architecture and microstructures–perspectives on a general kinematic model–a 'blueprint' for till development. Quat. Sci. Rev. 50, 105–124.
Menzies, J., van der Meer, J.J., Rose, J., 2006. Till—as a glacial "tectomict", its internal architecture, and the development of a "typing" method for till differentiation. Geomorphology 75 (1), 172–200.
Menzies, J., van der Meer, J.J.M., Ravier, E., 2016. A kinematic unifying theory of microstructures in subglacial tills. Sediment. Geol. 344, 57–70.
Murray, T., Dowdeswell, J.A., 1992. Water throughflow and the physical effects of deformation on sedimentary glacier beds. J. Geophys. Res. Solid Earth 97 (B6), 8993–9002.
Murray, T., Porter, P.R., 2001. Basal conditions beneath a soft-bedded polythermal surge-type glacier: Bakaninbreen, Svalbard. Quat. Int. 86 (1), 103–116.
Ó Cofaigh, C., Evans, D.J., Hiemstra, J.F., 2011. Formation of a stratified subglacial 'till'assemblage by ice-marginal thrusting and glacier overriding. Boreas 40 (1), 1–14.
Ouchiyama, N., Rough, S.L., Bridgwater, J., 2005. A population balance approach to describing bulk attrition. Chem. Eng. Sci. 60 (5), 1429–1440.
Peters, J.F., Muthuswamy, M., Wibowo, J., Tordesillas, A., 2005. Characterization of force chains in granular material. Phys. Rev. E 72 (4), 041307.
Phillips, E., Merritt, J., 2008. Evidence for multiphase water-escape during rafting of shelly marine sediments at Clava, Inverness-shire, NE Scotland. Quat. Sci. Rev. 27, 988–1011.
Piotrowski, J.A., Larsen, N.K., Menzies, J., Wysota, W., 2006. Formation of subglacial till under transient bed conditions: deposition, deformation, and basal decoupling under a Weichselian ice sheet lobe, central Poland. Sedimentology 53 (1), 83–106.
Powers, M.C., 1953. A new roundness scale for sedimentary particles. J. Sediment. Petrology 23, 117–119.
Price, R.J., 1970. Moraines at Fjallsjökull, Iceland. Arct. Alp. Res. 2, 27–42.
Reinardy, B.T., Hiemstra, J.F., Murray, T., Hillenbrand, C.D., Larter, R.D., 2011. Till genesis at the bed of an Antarctic Peninsula palaeo-ice stream as indicated by micromorphological analysis. Boreas 40 (3), 498–517.
Roberts, D.H., Hart, J.K., 2005. The deforming bed characteristics of a stratified till assemblage in north East Anglia, UK: investigating controls on sediment rheology and strain signatures. Quat. Sci. Rev. 24 (1), 123–140.
Rose, K.C., Hart, J.K., 2008. Subglacial comminution in the deforming bed: inferences from SEM analysis. Sediment. Geol. 203, 87–97.
Sane, S.M., Desai, C.S., Jenson, J.W., Contractor, D.N., Carlson, A.E., Clark, P.U., 2008. Disturbed State constitutive modeling of two Pleistocene tills. Quat. Sci. Rev. 27 (3), 267–283.
Sharp, M.J., 1984. Annual moraine ridges at Skálafellsjökull, southeast Iceland. J. Glaciol. 30, 82–93.
Sharp, M., Gomez, B., 1986. Process of debris comminution in the glacial environment and implications for quartz sand-grain micromorphology. Sediment. Geol. 46, 33–47.
Sigurðsson, O., 1998. Glacier variations in Iceland 1930-1995. Jökull 45, 3–25.
Skempton, A.W., 1964. Long-term stability of clay slopes. Geotechnique 14, 77–102.
Smith, A.M., Murray, T., Nicholls, K.W., Makinson, K., Aðalgeirsdóttir, G., Behar, A.E., Vaughan, D.G., 2007. Rapid erosion, drumlin formation, and changing hydrology beneath an Antarctic ice stream. Geology 35 (2), 127–130.
Tembe, S., Lockner, D.A., Wong, T.F., 2010. Effect of clay content and mineralogy on frictional sliding behavior of simulated gouges: binary and ternary mixtures of quartz, illite, and montmorillonite. J. Geophys. Res. Solid Earth 115 (B3).
Thomason, J.F., Iverson, N.R., 2006. Microfabric and microshear evolution in deformed till. Quat. Sci. Rev. 25 (9), 1027–1038.
Trommelen, M.S., Ross, M., Ismail, A., 2014. Ribbed moraines in northern Manitoba, Canada: characteristics and preservation as part of a subglacial bed mosaic near the core regions of ice sheets. Quat. Sci. Rev. 87, 135–155.
Truffer, M., Harrison, W.D., Echelmeyer, K.A., 2000. Glacier motion dominated by processes deep in underlying till. J. Glaciol. 46 (153), 213–221.
Tulaczyk, S., Kamb, W.B., Engelhardt, H.F., 2000. Basal mechanics of Ice Stream B, West Antarctica 1. Till mechanics. J. Geophys. Res. 105 (B1), 463–482.
Voivret, C., Radjai, F., Delenne, J.Y., El Youssoufi, M.S., 2009. Multiscale force networks in highly polydisperse granular media. Phys. Rev. Lett. 102 (17), 178001.
van der Wateren, F.M., 1995. Structural Geology and Sedimentology of Push Moraines. - processes of soft sediment deformation in a glacial environment and the distribution of glaciotectonic styles. Meded. Rijks Geol. Dienst 54, 1–168.
Woodward, J., Murray, T., Clark, R.A., Stuart, G.W., 2003. Glacier surge mechanisms inferred from ground-penetrating radar: Kongsvegen, Svalbard. J. Glaciol. 49 (167), 473–480.